NTNU – Trondheim
Norwegian University of
Science and Technology

Initial Growth of $LaFeO_3$ on (111)-Oriented Substrates

Jon Vegard Wasvik

Master of Science in Electronics
Submission date: June 2013
Supervisor: Thomas Tybell, IET

Norwegian University of Science and Technology
Department of Electronics and Telecommunications

Project Description

Over the last 20 years, advancement in physical deposition has led to the development of epitaxial all oxide systems, opening for combining epitaxially thin films of different crystalline oxides to form artificial materials. More recently it has become evident that interfaces between epitaxial thin films can carry functionality of its own. However, one prerequisite is a high degree control of thin film surfaces and interfaces. Of special interest are interfaces between materials having different crystalline structure and orientation, however the development of such interface systems is a novel field.

The goal of this master thesis is to elucidate initial growth of (111)-oriented $LaFeO_3$ by pulsed laser deposition in order to control the surface properties of the materials system. In order for this the following question is to be addressed:

- How does the substrate material, comparing $SrTiO_3$ and $(La, Sr)MnO_3$, affect the initial growth of $LaFeO_3$?

Two sub-goals are also to elucidate the possible growth modes governing the synthesis of (111)-oriented $LaFeO_3$ thin films, and optimize how RHEED analysis can be used in-situ for such studies.

Abstract

Perovskite oxide thin films grown in the (111)-direction are, due to their expected novel properties resulting from the strong structural and electronic coupling, interesting for all oxide heterostructures. A prerequisite for such structures is control of growth and surface morphology. This work aims to elucidate the initial growth of $LaFeO_3$ on (111)-oriented $SrTiO_3$ and $La_{0.7}Sr_{0.3}MnO_3$ substrates in order to investigate any differences in growth induced by the substrates.

In this master thesis, initial growth of the antiferromagnet $LaFeO_3$ by Pulsed Laser Deposition has been investigated both on (111)-oriented $SrTiO_3$ and on three monolayer thick $La_{0.7}Sr_{0.3}MnO_3$ buffer layers, the materials have been chosen due to their magnetic coupling properties. Characterization has been done with Atomic Force Microscope, in-situ Reflection High-Energy Electron Diffraction (RHEED) and X-Ray Diffraction.

A study of the initial growth on $SrTiO_3$ is presented, showing two growth regimes over the first two monolayers. The first RHEED intensity peak is observed after half as many pulses as the next, the continued growth rate is 45 laser pulses per monolayer. In the case of $LaFeO_3$ grown on a $La_{0.7}Sr_{0.3}MnO_3$ buffer layer, the RHEED oscillations show a constant growth rate of 45 laser pulses per monolayer. A possible origin for the change in RHEED period has been identified as filling of $Sr-$ vacancies in the substrate surface.

Furthermore, in order to elucidate the continued growth of $LaFeO_3$, thicker films between 2.5 and $30nm$ are grown. They show an initial layer-by-layer growth mode over the first $2.5nm$ before transitioning into 3D island growth mode. $LaFeO_3$ was also seen to grow smoother at low temperatures ($540°C$).

The (111)-oriented $LaFeO_3/La_{0.7}Sr_{0.3}MnO_3$ interface is interesting as it exhibit exchange coupling in the (100)-oriented interface and an increased coupling is expected in the (111)-orientation. $LaFeO_3$ $/La_{0.7}Sr_{0.3}MnO_3$ heterostructures are synthesized in order to investigate the growth at a rougher interface. The films showed a good crystalline quality, but due to early roughening they had a near 3D surface at the interface and a 3D surface in the end.

In-situ measurements of the surface in-plane constant showed a large change in all films were it was applied, this was attributed to a general roughening effect leading to an increased angular distribution of the RHEED beam.

These investigations are important for further understanding of growth in the (111)-orientation and in preparation for further investigations of the $LaFeO_3/La_{0.7}Sr_{0.3}MnO_3$ interface coupling.

Sammendrag

Perovskitt oksid tynnfilmer vokst i (111) retningen er på bakgrunn av sine forventede nye egenskaper som oppstår som et resultat av sterke strukturelle og elektroniske koblinger interessante for heterostrukturer bestående utelukkende av oksider. En forutsetning for denne typen strukturer er kontrollert vekst og morfologi. Dette arbeidet har som målsetning å belyse initiell vekst av $LaFeO_3$ på (111) orienterte $SrTiO_3$ og $La_{0.7}Sr_{0.3}MnO_3$ substrater for å undersøke eventuelle forskjeller i veksten indusert av substratene.

I dette studiet har initiell vekst av antiferromagnetisk $LaFeO_3$ ved pulserende laser deponering blitt undersøkt både på (111) orientert $SrTiO_3$ og på tre monolag tykke $La_{0.7}Sr_{0.3}MnO_3$ bufferlag, materialene er valgt på bakgrunn av deres magnetiske koblings egenskaper. Karakterisering har blitt gjort med atomærkraftmikroskopi, in-situ refleksjons høy-energi elektrondiffraksjon (RHEED) og røntgenstrålediffraksjon.

En studie av initiell vekst på $SrTiO_3$ er presentert og viser to vekst regimer i løpet av de to første monolagene. Den første RHEED intensitet-toppen er observert etter halvparten så mange pulser som den neste, den påfølgende vekstraten er 45 laser pulser per monolag. For $LaFeO_3$ vokst på $La_{0.7}Sr_{0.3}MnO_3$ buffer lag, viser RHEED oscillasjonene en konstant vekstrate på 45 laser pulser per monolag. En mulig opprinnelse på endringen i RHEED perioden har blitt identifisert som fylling av $Sr-$ hull i substrat overflaten.

Deretter, for å belyse den videre veksten av $LaFeO_3$ er tykkere filmer mellom 2.5 and $30nm$ vokst. De viser en initiell lag-etter-lag vekst for de første $2.5nm$, før en overgang til 3D øyvekst er observert. Jevnere vekst av $LaFeO_3$ ble videre observert for lave temperaturer ($540°C$).

Grensesjikt til (111) orientert $LaFeO_3/La_{0.7}Sr_{0.3}MnO_3$ er interessant siden det viser en utvekslingskobling mellom elektronene i (100) orienterte grensesjikt og er forventet å ha en sterkere kobling i (111) orienteringen. $LaFeO_3$ $/La_{0.7}Sr_{0.3}MnO_3$ heterostrukturer er vokst for å undersøke vekst på en røffere overflate. Filmene hadde god krystallinsk kvalitet, men på grunn av tidlig økning i ruhet hadde de en morfologi nær 3D ved grensesjiktet og 3D til slutt.

In-situ målinger viste også en stor endring for i plan gitterkonstanten for alle filmer der det ble målt, dette ble antatt å være som følge an en generell økning i røffhet som øker den angulære dispersionen til RHEED strålen.

Disse undersøkelsene er viktige for å danne en forståelse for (111) orientert vekst og som en forberedelse for videre undersøkelser av koblingen i $LaFeO_3/La_{0.7}Sr_{0.3}MnO_3$ grensesjiktet.

Preface

This master thesis has been carried out at the Institute of electronics and telecommunications at the Norwegian University of Science and Technology (NTNU), in the spring of 2013. It is submitted as the final part of my Master of Science in Electronics. The experimental work has been done in the laboratories of the Oxide Electronics Group.

First, I would like to award a special thanks to my supervisor Prof. Thomas Tybell for giving me the opportunity to do research in the exciting field of oxide electronics. His patience and infectious passion for the field has been a huge inspiration.

Also, I would like to thank my co-supervisor Ingrid Hallsteinsen and Erik Folven for valuable discussions and help with keeping the instruments up and running.

Jon Vegard Wasvik
NTNU, Trondheim
June 30, 2013

Contents

1 Introduction **2**

2 Theory **6**
2.1 Exchange Bias 6
2.1.1 Exchange Bias in Transition Metal Oxides 8
2.2 Growth Mode 10
2.2.1 Growth in Thermodynamic Equilibrium 11
2.2.2 Kinetic Growth 11
2.2.3 Frank-Van der Merwe (layer-by-layer) 11
2.2.4 Volmer-Weber (island) 12
2.2.5 Stranski-Krastanov 12
2.2.6 Step Flow 12
2.2.7 Strain 12
2.3 Transition Metal Oxide Growth 13
2.3.1 The (111)-oriented Substrate 13
2.3.2 Growth Studies on (111)-oriented Substrates 14
2.4 The Materials System 17
2.4.1 $SrTiO_3$ (Strontium Titanate) 17
2.4.2 $LaFeO_3$ (Lanthanum Ferrate) 17
2.4.3 $La_{0.7}Sr_{0.3}MnO_3$ (Lanthanum Strontium Manganite) 19

3 Experimental **20**
3.1 Substrate Preparation Procedure 20
3.2 Pulsed Laser Deposition 21
3.3 Reflection High-Energy Electron Diffraction 23
3.3.1 Basic principle 24
3.3.2 RHEED Diffraction Pattern 25
3.3.3 RHEED Intensity and Growth Modes 26
3.3.4 In-Plane Lattice Spacing (d-spacing) 27
3.4 X-ray Diffraction 28
3.5 Atomic Force Microscope 31

4 Results and Discussion **34**
4.1 Substrate Preparation 34
4.1.1 Substrate Results 34
4.1.2 Substrate Discussion 37
4.2 Initial Growth 39
4.2.1 Ultrathin Growth of LFO on STO 39
4.2.1.1 Discussion 45
4.2.2 Ultrathin Growth of LFO on LSMO 48
4.2.2.1 Discussion 51
4.3 Thick Growth 53
4.3.1 LFO on STO 53
4.3.1.1 Discussion 59
4.3.2 Heterostructures - LFO/LSMO 62
4.3.2.1 Discussion 67

5 Conclusion **70**

6 Further Work **72**

Chapter 1

Introduction

Motivation During the past 40 years the unprecedented development of the semiconductor industry has led to a doubling of transistors per square area every two years. Such a development was first predicted by Moore in 1965 [1] (later adjusted in 1975 [2]) and has held up ever since. However, the constant field scaling of the transistor has come to an end. Moore's law still holds, but the relation between transistor area, processing speed and power consumption is changing and resulting in novel ways in which to increase performance [3].

In memory technology magnetism has played an important role ever since the 1940's, and more so after the discovery of the spin dependent resistance known as Giant Magneto Resistance (GMR) in 1988 [4]. The GMR effect was further exploited with the introduction of the spin-valve, where two ferromagnetic layers are separated by a conducting non-magnetic layer. The magnetic field of one of the ferromagnetic layers is kept fixed and the other free to flip. Also, a similar concept is being used in the Magnetic Tunnel Junction (MTJ) where two ferromagnets are separated by a thin insulating non-magnetic layer. The insulating layer is thin enough for the electrons to tunnel through, due to quantum tunneling. The probability of tunneling is spin dependent and the orientation of the two ferromagnets magnetic fields may be used to control the probability of tunneling. The MTJ is already being used in Magnetic Random Access Memory (MRAM) in industry today [4].

In both the above mentioned structures one of the ferromagnets needs to be pinned while the other remains free to switch the magnetization. This is achieved through an effect known as the exchange bias [5]. At the interface between an antiferromagnetic and a ferromagnetic material an exchange anisotropy lead to a shift in the hysteresis loop and serves to pin the layer (A more detailed explanation may be found in section 2.1).

Transition Metal Oxides (TMO) offer exciting opportunities for the electronics industry as their highly correlated electrons leads to a range of phenomena such as metal-insulator transitions, superconductivity, multiferroics and Mott insulators [6]. Their structure also allows for the possibility to engineer specific properties by changing cationic species located at the A- and B- sites of their perovskite structure. Also the

perovskite magnetic structures are good materials for exchange bias. Their magnetic properties may be changed by cation substitution and magnetically different materials have similar lattice constants allowing for epitaxial growth [7]. Over the last two decades the research and interest in TMO's and their interfaces has flourished as new deposition techniques such as pulsed laser deposition (PLD) have surfaced [6, 8, 9, 10].

Especially interesting is growth of TMO's in uncommon crystallographic directions such as the (111)-direction. At such interfaces three oxygen atoms of the oxygen octahedral are shared whereas only one is shared over the (100)-interface [11]. This is expected to yield stronger electronic and structural coupling at the interface. The most prominent example up until today may be the unexpected observation of exchange bias at the paramagnetic-ferromagnetic interface of (111)-oriented $LaNiO_3(LNO)/LaMnO_3(LMO)$ superlattices [12].

Going back to the challenges faced by the semiconductor industry, TMO's may be a future valuable addition to keep the development going. The gate dielectric of the semiconductor transistor has already been replaced by a hafnium-based high k oxide dielectric and further incorporation of other oxides are expected [13]. In memory technology, exchange bias still play an important role, and further incorporation into more complex technologies such as spin-transfer torque MRAM (STT-MRAM) is expected [14].

In this work initial growth of $LaFeO_3$ (LFO) on (111)-oriented $SrTiO_3$ (STO) and $La_{0.7}Sr_{0.3}MnO_3$ (LSMO) is studied. The interface between the G-type antiferromagnetic material LFO and the ferromagnetic material LSMO is interesting for (111)-oriented exchange bias studies. At the interface the G-type antiferromagnetic spins are aligned parallel (uncompensated) which is expected to lead to a stronger pinning. Such an increase in pinning has been observed leading to an increase in the metal-insulator transition temperature in $La_{0.55}Pb_{0.45}MnO_3(LPMO)$/LFO bilayers [15]. A prerequisite for incorporation of TMO structures in future electronic devices is control of growth and surface morphology. The focus of this study is therefore the initial growth and the development of the governing growth mode.

Outline Following this introduction is a theory chapter in which the theoretical background of some of the effects and theories used in this master thesis will first be explained. First an introduction to the exchange bias anisotropy will be given, then a review of the different growth modes of TMO thin films will be presented as well as an introduction to strain in epitaxial thin films. Thereafter, a short introduction to some of the properties of the materials used in this work will be given. Finally, a review of some of the most important work on (111)-oriented TMO growth will be presented.

In the next chapter the deposition and characterization methods applied in this work will be described. Included is also descriptions of how the different methods have been used in this study.

In chapter 4, the results will be presented and discussed. This chapter has been divided into three sections; (4.1) the substrate properties, (4.2) the initial growth of LFO on STO and LSMO buffer layers and (4.3) the continued growth of LFO and

LFO/LSMO heterostructures.

Finally, the conclusions of this study will be given, followed by a presentation of some thoughts regarding possible future work.

Chapter 2

Theory

This chapter will present the theory motivating the work done in this study and the theory behind the experimental work.

One of the main motivations for this study is the exchange bias at antiferromagnetic/ferromagnetic interfaces. In order to understand the importance, utility and implications of such an effect a short theoretical introduction will be given in section 2.1 along with a few examples of exchange bias in TMO's.

Furthermore, the quality of TMO interfaces are strongly related to the growth mode during deposition of such films. The different growth modes of TMO thin films will therefore be introduced in section 2.2. Another important parameter which can have a large impact on the growth mode and interface effects is strain across the interface. Basic strain theory will thus also be explained in subsection 2.2.7.

A quick introduction to the materials used in this study will be given in section 2.4. The motivation behind this section is to clarify why these materials are chosen and to present their main properties.

The final part of this chapter concerns itself with presenting some of the relevant work done within (111)-oriented TMO growth. The motivation for such a chapter is to illuminate the state of the art and the motivation behind the research being done.

2.1 Exchange Bias

As mentioned above, the exchange bias is one of the main motivations behind the chosen material system investigated in this study. It's role in memory technology, shifting the hysteresis loop, has been (and still is) of great importance. For future use the exchange coupling is also interesting for other exchange anisotropy effects in addition to the loop shift, such as magnetic stabilization in magnetic materials approaching particle sizes leading to thermal random flipping of magnetic moment [16]. Its relevance is thus still very much maintained.

A ferromagnetic material will, bellow its Curie temperature (T_C), exhibit a residual magnetization when cooled under a static magnetic field. An antiferromagnetic mate-

rial, however, show no net magnetization. (A more precise definition of the two can be found in previous work [17]). The magnetization of a ferromagnet as a function of applied magnetic field, known as a hysteresis loop, is illustrated in figure 2.1a.

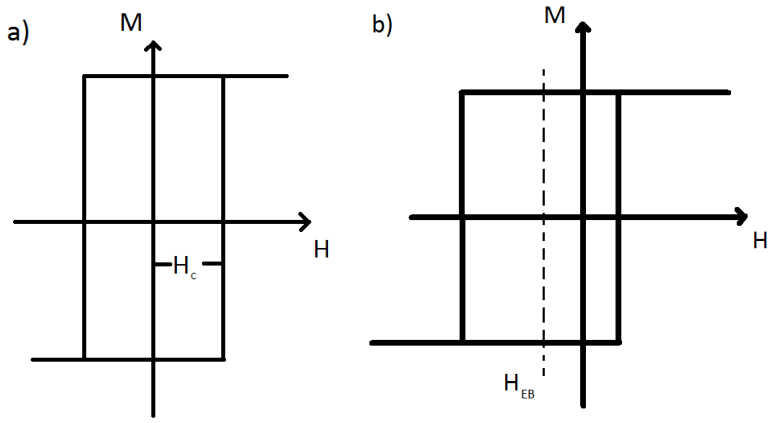

Figure 2.1: (a) Magnetization of a ferromagnet as a function of an applied magnetic field, known as a hysteresis loop. (b) Magnetization of a pinned ferromagnet. M is the magnetization, H is the applied magnetic field, H_C is the coercive field and H_{EB} is the exchange bias shift in the hysteresis loop.

In 1956 Meiklejohn and Bean discovered a magnetic anisotropy at the interface between antiferromagnetic and ferromagnetic materials [5]. This anisotropy is today known as the exchange bias and is extensively utilized in modern electronics. When a antiferromagnetic-ferromagnetic couple is field cooled from a temperature above the Néel temperature, but below the Curie temperature, to a temperature below the Néel temperature exchange anisotropy is observed at the interface [18]. The hysteresis loop is shifted away from the zero-field position as illustrated in figure 2.1b. This shift is known as exchange bias (H_{EB}) and is generally negative related to the cooling field (negative exchange bias) [19]. The coercive field, H_C, of the hysteresis loop is also seen to increase. Both the shift and the increased coercive field are seen to disappear at the Néel temperature, confirming that the antiferromagnetic layer is their origin [18].

The origin of the exchange anisotropy can be intuitively understood by considering a antiferromagnetic-ferromagnetic interface as illustrated in figure 2.2. Starting out by applying a magnetic field in the temperature range $T_N < T < T_C$, the spins of ferromagnetic material will align with the applied field, while the antiferromagnet spins remain disordered. When lowering the temperature below the Néel temperature ($T < T_N$) the antiferromagnetic spins at the interface will arrange ferromagnetically with the spins of the ferromagnet (a). The rest of the spins in the antiferromagnet will align antiferromagnetically. When the applied field is reversed the ferromagnetic spins will start to turn, but with a sufficiently large antiferromagnetic anisotropy the

spins in the antiferromagnet will not turn (b-c). The spins in the two materials at the interface will still try to align ferromagnetically, and a microscopic exchange coupling acts upon the ferromegnetic spins. The ferromagnetic spins thus have only one stable configuration (the anisotropy is unidirectional), and a higher field needs to be applied to reverse the spins in the ferromagnet. Since the spins have to overcome the exchange coupling exerted from the antiferromagnetic spins, the field needed to completely reverse the ferromagnetic spins is larger, and the coercive field on the negative side will increase. On the other hand, when the magnetic field returns to the positive values, the antiferromagnetic spins will exert a torque on the ferromagnetic spins in the same direction as the field (d). The coercive field on the positive side will thus decrease. The final result is a shift in the hysteresis loop along the magnetic field axis. [18, 20]

If the spin alignment at the interface is ferromagnetic, the exchange field is negative and the loop shift will shift opposite to the cooling field. However, if the coupling at the interface is antiferromagnetic, the exchange field is positive and the loop is shifted with the cooling field. [19]

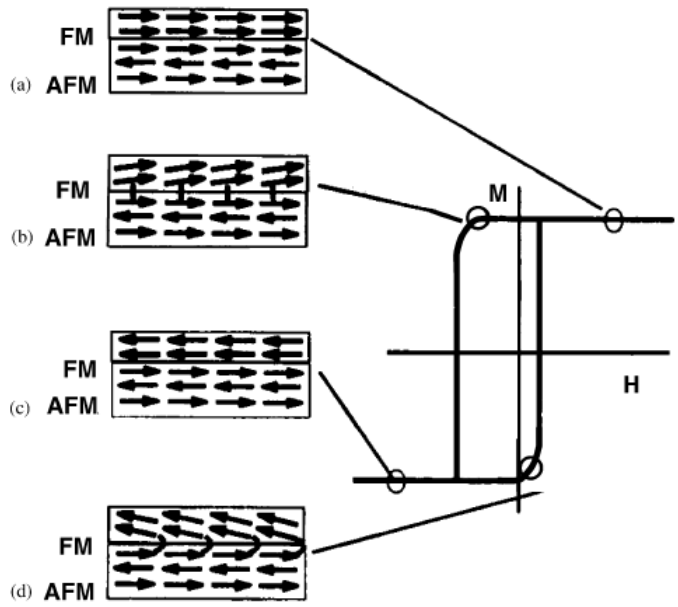

Figure 2.2: Schematic diagram of the spin configuration of an ferromagnetic-antiferromagnetic couple at the different stages of a shifted hysteresis loop for a negative exchange bias. Reproduced from [20]

2.1.1 Exchange Bias in Transition Metal Oxides

The materials in this study are chosen to gain knowledge about (111)-oriented growth in general, but more specifically to investigate the growth at the interface between ma-

terials making up a model system for exchange bias in (111)-oriented TMO's. LFO is a G-type antiferromagnet and thus has a parallel arrangement of spins in the (111) plane. Also, (111)-oriented TMO interfaces share three instead of one oxygen atom from the oxygen octahedral. This is expected to lead to a stronger structural and electronic coupling and make growth in this direction interesting [12]. TMO interfaces demonstrating exchange bias and an unexpected exchange bias effect between a paramagnetic and a ferromagnetic material at a (111)-oriented material will here be presented.

Exchange bias in $La_{0.67}Sr_{0.33}MnO_3/SrRuO_3$(SRO) bilayers has been reported in several articles [7, 19]. Ke et al [7, 19] report on antiferromagnetic/positive exchange bias at this ferromagnetic-ferromagnetic interface. During field pinning measurements the magnetization loops were shifted along the field axis in the same direction as the pinning field, this give a clear indication of an antifferomagnetic coupling between the layers. The exchange field is also seen to be independent of the order of the layers. In addition, the coercivity is larger for $La_{0.67}Sr_{0.33}MnO_3$ on top compared to SRO on top, attributed to a large lattice mismatch inducing higher coercivity in $La_{0.67}Sr_{0.33}MnO_3$. Also, during field cooling measurements the exchange field saturates for large cooling fields further confirming the exchange anisotropy.

In LSMO/SRO superlattices inverted hysteresis and giant exchange bias has been reported [21]. Magnetic hysteresis loops recorded at low temperatures show a inversion of the central hysteresis part. The magnetically soft LSMO layers reverse first, followed by reversion of the magnetically hard SRO layers at opposite polarity, as expected. At higher temperatures however; the central hysteresis part is normal but the magnetically hard SRO layer switch first when reducing the magnetic field from saturation, which is unconventional. This was by Ziese et al [21] attributed to the interplay of magnetocrystalline anisotropy energy, antiferromagnetic exchange coupling strength and interfacial Bloch wall width.

The (111)-oriented interfaces offers exciting new possibilities due to its polar discontinuity and the most prominent until now may be the observation of exchange bias in (111)-oriented LNO/LMO superlattices [12]. LNO is a paramagnetic material and LMO is a ferromagnet, exchange bias is thus not expected at such an interface. When field cooling in a 0.4T field, the hysteresis loop was seen to shift in the direction of negative fields. On the other hand, when field cooling under -0.4T the loop shifted in the other direction. This is a clear exchange bias behavior and confirms the observation of exchange bias at the (111)-oriented LNO/LMO interface at low temperatures (5K).

These observation of unconventional effects and the expectations of novel properties at (111)-oriented interfaces makes growth of heterostructures and superlattices in this direction attractive. To be able to synthesize these structures, control of growth is first needed and therefore the focus of this work.

2.2 Growth Mode

As TMO thin films are to be utilized in electronic devices, epitaxial growth and smooth surfaces and interfaces are prerequisites [22]. The control of surface morphology is therefore an important aspect of thin film growth. In order to achieve this it is important to have a good understanding of the different growth modes and how they can be influenced. In this section different models of thin film growth are presented.

The scope of this discussion will be limited to epitaxial growth. Epitaxy refers to the growth of one crystal on another crystal where the crystal structure is extended over the interface [10]. The most basic being homoepitaxy, where a material deposited is the same as the substrate. In heteroepitaxy on the other hand, the material deposited is different from the substrate material. Also, a step-and-terrace surface will be assumed. During thin film growth there are several processes happening at the surface, including: absorption, diffusion and nucleation. Absorption is the process of the adatoms arriving at the surface, diffusion is the adatoms moving along the surface and nucleation is the adatoms settling in their final position. The growth modes can be categorized into four main modes: layer-by-layer (Frank-Van der Merwe), island (Volmer-Weber), Stranski-Krastanov and step flow. To understand what constitutes each of the modes a combination of thermodynamics and kinetics may be applied.

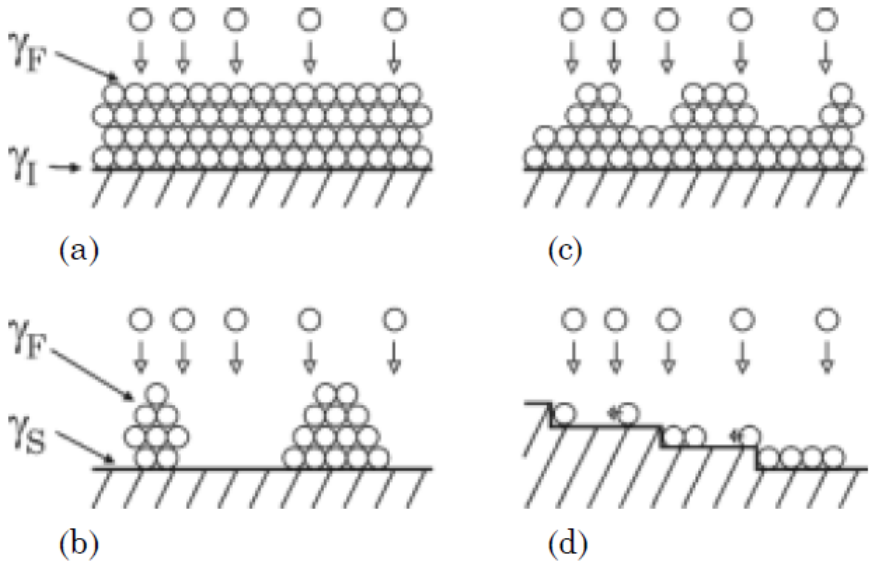

Figure 2.3: Film growth modes: Frank-Van der Merwe (layer-by-layer) (a), Volmer-Weber (3D island) (b), Stranski-Krastanov (c) and step flow (d). Reproduced from [22]

2.2.1 Growth in Thermodynamic Equilibrium

In thermodynamic equilibrium the adatoms arriving at the surface will have a diffusivity, D, and keep moving across the surface until they encounter an energetically favorable site [23]. On a perfect surface (free from defects) these sites will be where the adatoms increase their atomic coordination, leading to a nucleation where adatoms collide and at step-edges. In the thermodynamic approach the development of the surface morphology will depend on the binding energy of the adatoms. Considering the free energy of the film surface (γ_F), substrate surface (γ_S) and the interface between film and substrate (γ_I), three different growth modes are possible. Depending on the relation between the three factors, the adatoms will nucleate in one of the three following growth modes: layer-by-layer, Volmer-Weber or Stranski-Krastanov.

2.2.2 Kinetic Growth

In a vapor-phase deposition system such as PLD, the film growth rarely happens under thermodynamic equilibrium [22]. The diffusion of the adatoms at the surface is limited and they can no longer always diffuse until they find an energetically favorable position. The average distance an adatom can diffuse is now limited by a diffusion length, l_D, and the adatom will nucleate within this distance. Adatoms deposited on an island have a tendency to transport to a lower layer in order to increase their atomic coordination, as mentioned above. This is known as interlayer transport and is the diffusion of an atom to a lower terrace. However, depending on the type of bonding the probability of such a jump to a lower level may be reduced. This is due to the unfavorable position at the edge which creates a barrier known as the Ehrlich-Schwoebel barrier (ES-barrier) [24, 25]. A large ES-barrier will immediately lead to 3D island growth as the adatoms are unable to diffuse to lower levels and thus are forced to nucleate and create new islands. [23]

2.2.3 Frank-Van der Merwe (layer-by-layer)

In this growth mode a complete layer is grown before any significant nucleation of islands on the next layer occur, as illustrated in figure 2.3a. The circumstances for this growth mode can be explained by a reduction in surface energy and occur when the following equation is satisfied:

$$\gamma_I + \gamma_F \leq \gamma_S \tag{2.1}$$

This mode is favored for low misfit growth (meaning comparable lattice parameters in substrate and film) and for low interface energy (low film surface energy and high substrate surface energy) which leads to a strong bonding between the film and the substrate [26]. In other words, it is energetically favorable for the adatoms to nucleate at the growing layer, as opposed to start forming a second layer. Elastic strain will also influence the energy balance as the film grows thicker, the energy at the interface (γ_I) will thus need to be replaced by γ_{IN}, where N is the number of monolayers.

2.2.4 Volmer-Weber (island)

In the opposite situation, equation 2.1 is not fulfilled and we have Volmer-Weber growth mode. Also known as island growth, Volmer-Weber occur when it is more energetically favorable for the adatoms to nucleate and form new islands instead of nucleating at the film surface and complete the layer. Islands will then form at the interface as illustrated in figure 2.3b. An adatom bound to the surface has a lower energy than the substrate itself. [22]

2.2.5 Stranski-Krastanov

In this growth mode the growth starts out with layer-by-layer growth, but changes to island growth after a certain number of monolayers as illustrated in figure 2.3c. This is believed to happen as a consequence of the increasing stress and subsequent strain relief [26]. In the beginning stages it is energetically favorable to nucleate at the substrate and complete the layer, but after a while the strain increase and, ultimately, relaxation occur. [22]

2.2.6 Step Flow

If the diffusion-length is larger than the terrace-length and the interlayer mass transport is fast it will lead to step flow as illustrated in figure 2.3d. The adatoms will then diffuse to the step edge and nucleation at the terraces is prevented. The steps will then propagate giving rise to step flow. However, if the deposition is not uniform, the steps may propagate at different velocities and give rise to step bunching. [22]

2.2.7 Strain

To achieve a high quality crystalline film the materials need to have similar structure and parameters. If the deposited material have similar lattice parameters as the substrate, as shown in figure 2.4a, strained growth is achievable. If the mismatch is larger there are two possibilities; either the film will grow with the same in-plane lattice parameter as the substrate or it will relax to its own lattice parameter, as seen in figure 2.4b and c. A strained epitaxial film is likely to happen when the lattice of the material is slightly larger (or smaller) than the substrate and the relaxation when it is much larger (or smaller). Thin films grown under strain will normally have a relaxation thickness were the lattice returns to bulk lattice parameters.

The likelihood of these three cases may be calculated by using the following formula for mismatch f [10]:

$$f = \frac{2(a_f - a_s)}{a_f + a_s} \sim \frac{a_f - a_s}{a_s} \tag{2.2}$$

Where a_f and a_s correspond to the lattice parameters of the film and the substrate. For epitaxial growth to happen the mismatch should not be higher than 10% ($f = 0.1$) or the interfacial bonds will not align and epitaxial growth cannot happen [10].

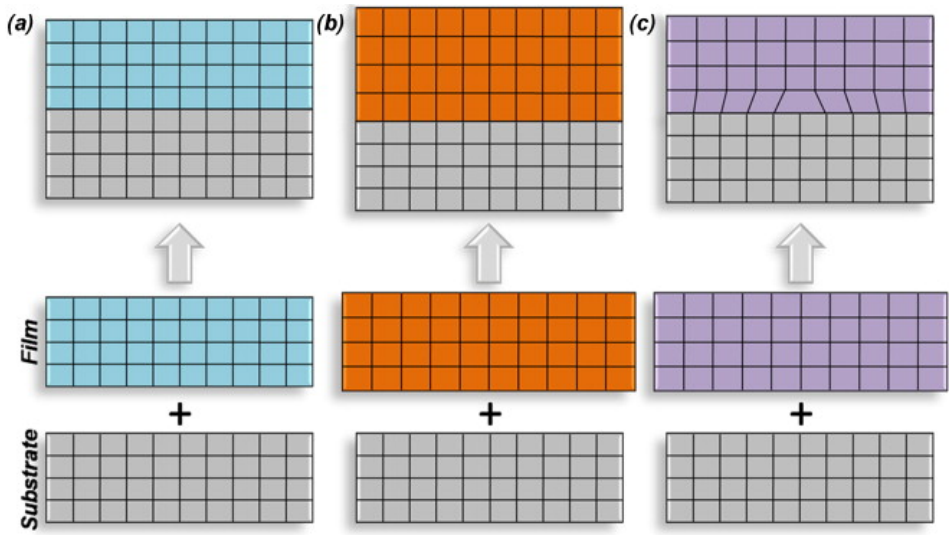

Figure 2.4: Schematic illustration of (a) a nearly perfectly lattice matched, (b) strained and (c) relaxed heteroepitaxial film growth. Reproduced from [10]

2.3 Transition Metal Oxide Growth

TMO's grown on (111)-oriented substrates is largely an undeveloped area. During the last decade the interest has however been increasing and more and more articles are published on the matter. The first subsection deals with the challenges with the (111)-oriented substrate, whereas the following subsection review some of the most important work done on growth of (111)-oriented TMO. For broader review of (111)-oriented growth and a review of LFO thin films see previous work [17].

2.3.1 The (111)-oriented Substrate

The first thing to consider for growth of TMO's on any substrate with any orientation is the substrate surface. The control of the substrate surface has long been a challenge for growth on (111)-oriented STO. Blok et al [27] defined three main criteria for a good surface: " (1) single termination; (2) a stable interface with air/vacuum without major reconstructions and (3) a stable interface with the film material.". All of the above poses problems for growth on (111)-oriented STO. Ti-rich substrate surfaces have been reported [28, 29], and Ti^{4+} termination is assumed in this study. But, even if single

termination is achieved, surface reconstructions on the surface prevents coherent growth and may lead to disrupted or intermixed interfaces manifested as rougher growth over the first few monolayers. Also, the polar surface leads to incoherent growth and a polar catastrophe at the interface. A polar catastrophe at the interface is solved at the interface by one of two possibilities [30]; either by intermixing of atoms at the interface or by movement of electrons (possible with multivalence atoms present) [27]. A possible way of avoiding this problems is to introduce a metallic layer to screen the polar surface [27]. A free charge may screen, and thus stop, the polar catastrophe. It may also restore the reconstructed interface to its bulk termination or simply prevent reconstruction in the first place. Preparation methods using buffered HF giving a single termination has been reported by Biswas et al and Chang et al [29, 28].

2.3.2 Growth Studies on (111)-oriented Substrates

SRO is one of the few materials reported to grow in a 2D growth mode on (111)-oriented STO, owing to its metallic nature. Chang et al [31] reported on 2D growth of SRO where the governing growth mode was manipulated by growth temperatures and growth rate. They divided the initial growth into two growth regimes: regime 1, from 0 to 9 monolayers and regime 2, from 9 to 18 monolayers as illustrated in figure 2.5. At $700°C$, the first 4 monolayers grow in a layer-by-layer manner before a period of 6 monolayers grow in a 3D island growth mode (regime 1) as seen in figure 2.5a. The first RHEED intensity oscillation is absent, which is believed to be because of terminating layer conversion. After the first 9 monolayers the growth mode switches to a layer-by-layer growth mode in regime 2. By increasing the temperature to $800°C$ the layer-by-layer growth mode is observed from the first unit cell (regime 1) until an unidentified roughening starts at the 9th monolayer, characterized by dampening of RHEED intensity and lack of intensity recovery, as seen in figure 2.5b. It is thus seen that a layer-by-layer growth may be tuned by varying the growth temperature. In addition, adjusting the growth rate by varying the pulse repetition had a similar effect. An increased growth rate at $800°C$ resulted in a suppressed layer-by-layer growth mode in regime 1, but prevails in regime 2. At $700°C$ a decrease in growth rate leads to a layer-by-layer growth mode in regime 1 and a damped layer-by-layer growth mode in regime 2. The possibility of tuning the layer-by-layer growth over a wide range of thicknesses make SRO a good candidate for atomic-level sharp interface heterostructures.

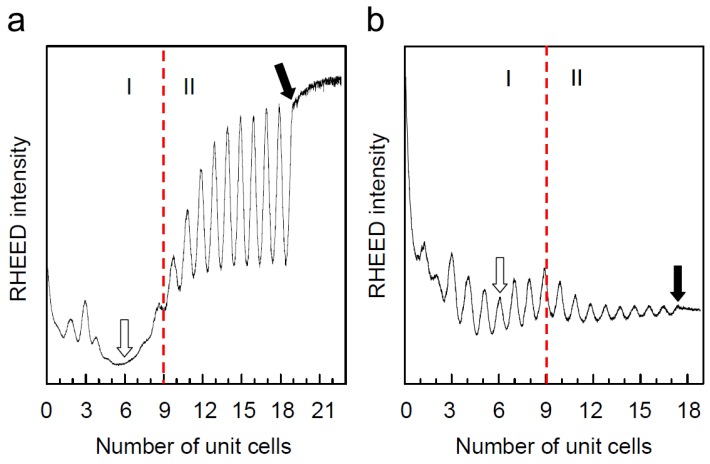

Figure 2.5: RHEED intensity curve from SRO deposited on (111)-oriented STO. The two growth regimes are marked by a line. The deposition temperatures are 700°C in (a) and 800°C in (b).

Initial growth of $SrFeO_{3-\delta}$ (SFO) directly on (111)-oriented STO substrates resulted in a completely damped RHEED intensity after three oscillations and 3D growth [32]. However, by introducing a SRO buffer layer, a layer-by-layer growth was achieved for a far-extended thickness range. This observation was done by Chang et al [32], and the initial roughening of SFO directly on STO is attributed to a electronic reconstruction-reduced electrostatic potential divergence (see figure 2.6). In addition, a 3D RHEED pattern was observed at deposition temperature of 800°C. This is attributed to low oxidation powers at growth temperatures above 650°C and thus an unstable environment for the Fe^{3+} terminating layer. During the growth of the SRO buffer layer, termination conversion from Ru^{4+} to $SrO_{2.5}^{3-}$ occurs, ruling out the formation of Fe-rich precipitates.

$BiFeO_3$ (BFO) has shown an enhanced spontaneous polarization on (111)-oriented STO compared to (001)-oriented STO, growth in this direction is thus interesting [33]. Blok et al [27] observed an almost instant 3D growth when depositing BFO on a (111)-oriented STO substrate. It seemed as if the wetting of the the film materiel was hampered by reconstruction at the surface. However, by first depositing a conducting metallic buffer layer of SRO the BFO film was observed to grow in a 2D growth mode for at least 10nm. This attributed to the screening of the polar surface by the metallic film.

Hallsteinsen et al [11] reports on the stability of growth of LSMO on (111)-oriented STO substrates prepared in DI water. At 700°C, the surface was seen to be unstable and became more disordered with thickness. The instability started already at 7nm and was attributed to an Asaro-Tiller-Grinfeld instability. In order to increase the surface

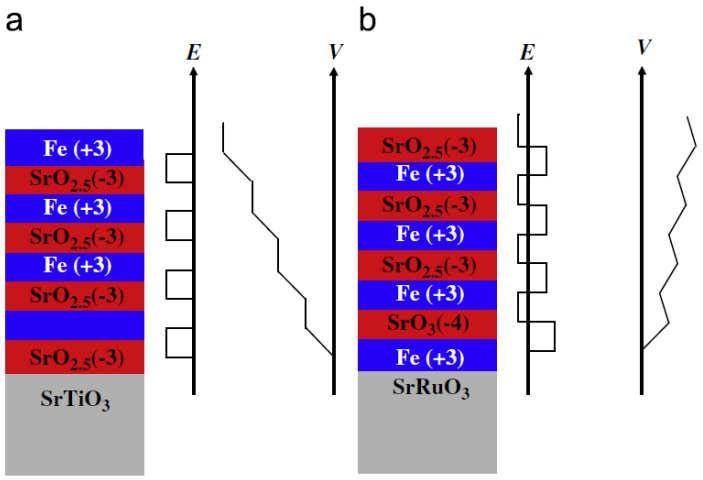

Figure 2.6: Illustration of the electrostatic polarity effect for SFO films grown on (a) an STO (111) substrate and on (b) an SRO buffer. The possible electric field (E) and potential (V) profiles are depicted. The charge profiles are depicted. The charge profiles are plotted according to an assumption that the oxygen non-stochiometric value is $\delta = 0.5$ except for the first SFO plane adjacent to the SRO, because the valence of the Fe ions persists at $+3$. On the first SFO plane only, the δ is assumed to be 0. The SRO buffer layer does not contribute to the electric potential , because free charge carriers compensate the electric field in the SRO. Reproduced from [32]

stability, thin films were grown at lower temperatures (500 and $600°C$) which reduce the adatom energy. For a deposition temperature of $500°C$, the surface was still seen to be smooth and the step-and-terrace structure showed a clear prolonging of the surface stability with falling temperature. At $500°C$, a 2D growth mode is first observed at ultrathin films below 1nm, then a 3D growth mode is observed $(0.5 - 4nm)$ before the surface again becomes smoother and, finally, returns to a unstable 3D growth mode (see figure 2.7). For higher temperatures the thinner films are seen to be smoother, whereas for low temperature the second 2D growth regime is seen to be larger. Thus, the thin film surface can be tuned by temperature to obtain the best film surface for the thickness wanted.

In conclusion It seems that growth on (111)-oriented surfaces is more easily achieved for materials with metallic properties such as SRO and LSMO. The growth mode may also to a large degree be manipulated by temperature and growth rate making it possible to use these materials as buffer- or bottom layers in heterostructures.

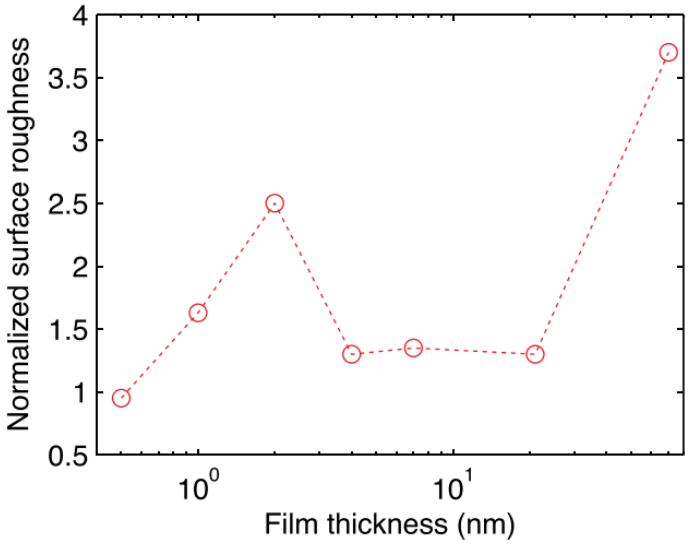

Figure 2.7: The surface roughness of LSMO films grown at $500°C$ normalized to the substrate roughness, versus film thickness. Reproduced from [11]

2.4 The Materials System

In this work LFO is grown on (111)-oriented STO substrates and LSMO. The combination of materials has been chosen due to their low lattice mismatch and their interesting spin orientation at the (111)-interface. Here, their material properties are summarized.

2.4.1 $SrTiO_3$ (Strontium Titanate)

$SrTiO_3$ (STO) is a popular choice as a substrate for perovskite thin film growth due to its low lattice mismatch with many transition metal oxides such as LSMO and LFO (0.69% for LFO and 0.87% for LSMO). In room temperature, STO has a cubic structure (Pm3m), and a lattice constant d = 3.905Å [34]. STO can be viewed as a stack of alternating charged Ti^{4+} and $(SrO)^{4-}$ layers along the (111)-direction. In (111)-oriented STO the distance between adjacent planes is 0.113nm, the distance between equivalent planes is $0.226nm$ and the in-plane lattice parameter is $0.552nm$, as illustrated in figure 2.8 [35]. In contrast to the non-polar surface of a (001)-oriented STO substrate, the (111)-oriented STO substrate has a polar surface [27].

2.4.2 $LaFeO_3$ (Lanthanum Ferrate)

$LaFeO_3$ is an interesting material due to its high Néel temperature of 740K originating from the large buckling angle in Fe-O-Fe bonds as illustrated in figure 2.9b. Its high Néel temperature makes it attractive for use in room temperature devices. It also has

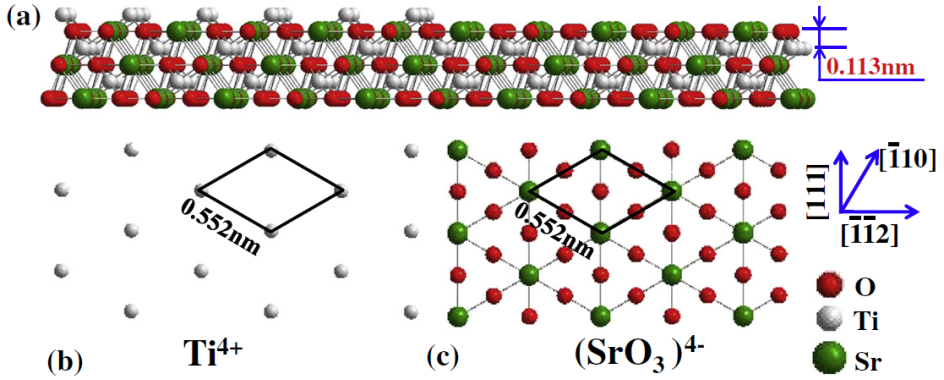

Figure 2.8: (a) The ball model of the STO (111) surface, (b) and (c) The corresponding top views of bulk truncated Ti^{4+} and $(SrO)^{4-}$ planes, respectively. The two dimensional unit cell in each plane is labeled. [35]

a G-type antiferromagnetic material below the Néel temperature, meaning that each spin is aligned antiparallel with the neighbor spins.

Structurally, LFO crystallize in a orthorhombic perovskite structure belonging to the Pbmn space group, with unit cell parameters of $a = 5.557\mathring{A}$, $b = 5.565\mathring{A}$ and $c = 7.854\mathring{A}$, at room temperature [36]. The unit cell can also be approximated by a pseudo-cubic unit cell of the ABO_3 perovskite structure, with a lattice constant of $d_{pc} = 3.93\mathring{A}$, marked with black in figure 2.9a [37]. The lattice mismatch with the STO substrate is thus 0.69% and will induce tensile strain in the thin film.

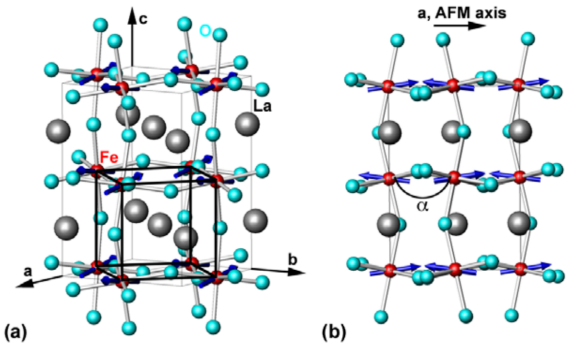

Figure 2.9: (a) Schematic drawing of the unit cell of LFO. The spins of Fe atoms (marked by small dark arrows) are oriented parallel to the a-axis of the orthorhombic unit cell. The perovskite unit cell drawn in black illustrates the epitaxial relationship. (b) (010) project of the unit cell. The buckling angle α is given by the Fe-O-Fe superexchange coupling. Reproduced from [37]

2.4.3 $La_{0.7}Sr_{0.3}MnO_3$ (Lanthanum Strontium Manganite)

$La_{0.7}Sr_{0.3}MnO_3$ (LSMO) is a half metallic ferromagnetic material with a Curie temperature of $\sim 370K$ [36]. It has a R-3c rhomboherdral symmetry with lattice constants $a = 5.51\mathring{A}$ and $c = 13.36\mathring{A}$ in hexagonal notation [34]. When viewed as a pseudo-cubic unit cell it has a lattice constant $d_{pc} = 3.88\mathring{A}$ and a distortion of 0.39 degrees [34]. When deposited on STO, a tensile strain of 0.6% is induced.

Chapter 3

Experimental

The focus of the following chapter is to explain the experimental methods utilized in this work. The substrate preparation procedure is first presented followed by an introduction to the growth system and the characterization tools.

3.1 Substrate Preparation Procedure

In previous work [17], growth of LFO and a LSMO/LFO heterostructure on DI-etched (111)-oriented substrates was successfully achieved. In this work two separate methods of preparation are used to prepare the substrates. Substrates are prepared using both de-ionized (DI) water and buffered hydrogen florid (HF) as etchant. The substrates used are $10x10mm$ (111)-oriented STO with one-side polish and a $0.1° \pm 0.1°$ miscut. The preparation procedure using DI-water is as follows:

- 5 minute cleaning in acetone, in ultrasonic bath
- 5 minute cleaning in ethanol, in ultrasonic bath
- Submerge 30 minutes in DI-water. Starting out at $70°C$ under ultrasonic vibration
- Dry with hydrogen (H_2) gas
- Anneal at $1200°C$ for 2 hours

The preparation procedure using HF acid is as follows:

- 5 minutes cleaning in acetone, in ultrasonic bath
- 5 minutes cleaning in ethanol, in ultrasonic bath
- 5 minutes submerged in DI-water. Starting out at $70°C$ under ultrasonic vibration
- Dry with H_2 gas

- Submerge 45 seconds in buffered HF (NH_4F:HF, 7:1)
- Clean for 1 minute in DI-water
- Clean for 5 minutes in DI-water
- Dry
- Anneal at 1050°C for 1 hour

The samples are cut into four equally sized pieces by a diamond cutter with a load of 75 gram and a rotation speed of 100 rpm. In preparation for deposition, the samples are cleaned ones more for 5 minutes in acetone and 5 minutes in ethanol under ultrasound sonication and dried with H_2 gas. Finally, they are glued to the sample holder using silver paste and annealed on a hot plate for 1 hour at 150°C.

The HF-preparation procedure was introduced in addition to the DI-preparation method used in previous work in order to obtain a higher quality substrate with higher reproducibility and elucidate any differences in film growth with the two methods.

3.2 Pulsed Laser Deposition

Pulsed Laser Deposition (PLD) is becoming one of the most popular deposition techniques for the growth of complex-oxide heterostructures, due to its atomic scale control, stochiometric transfer and simplicity [23, 38]. PLD is a physical vapor deposition technique were a pulsed laser is focused on the target material. The laser pulse vaporize the material upon impact and a plasma plume is formed. In figure 3.1, the laser plume during deposition of LFO (a) and LSMO (b) may be observed, the size of the plume will depend on the material and thus yield different deposition rates for identical lattice parameters. The material is then transported to the substrate surface by the plume. The setup, basic principle and main advantages are presented in a previous project [17].

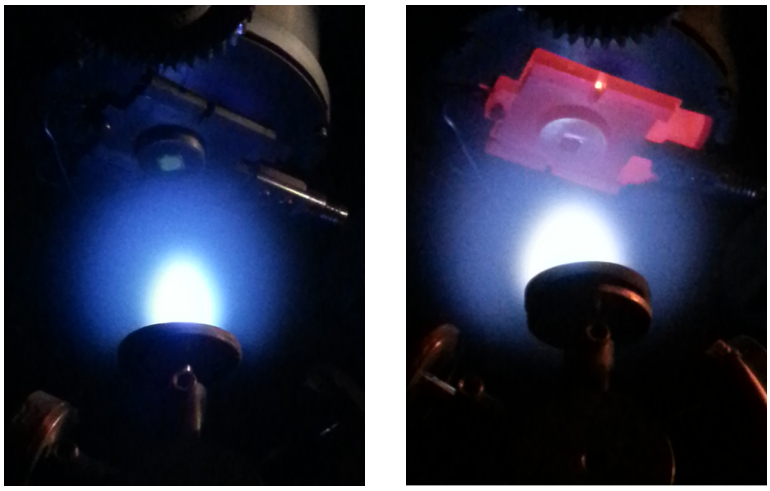

(a) (b)

Figure 3.1: Images of the plasma plume during deposition. (a) LFO and (b) LSMO

In this thesis the PLD system at the Oxide Electronics lab at NTNU has been used with the following process parameters:

- Excimer laser, wavelength = $248nm$
- Oxygen pressure: $0.35mbar$
- Target-substrate distance: $45mm$
- Laser energy: $1520mJ$ per pulse
- Laser pulse duration: $25ns$
- Pre-ablation parameters: 5 minutes at 5 Hz, 24 kV
- Laser deposition frequency: 1 Hz at 24 kV
- Scan area: 8x1 mm square
- Temperature set point: 540, 600 and $660°C$

In this work PLD has been used to grow 40 thin films of LFO and LFO/LSMO on (111)-oriented STO substrates. The film growth can be divided into two parts, ultrathin and thick films.

1. Ultrathin LFO thin films were grown on STO and LSMO buffer layers. On STO the LFO thin films were grown in two series. The first series consisted of approximately the following thin film thicknesses: 0.5, 0.9, 1.24 and 1.5 monolayer(s),

and the second series consisted of approximately the following thin film thicknesses: 0.25, 0.5, 0.75, 1.0 and 2.0 monolayer(s). Also, a series of sub-monolayer thick LFO thin films grown on 3 monolayer thick LSMO buffer layers were grown. These thin films had a LFO thickness of 0.5, 1.0, 1.5 and 2.0 monolayer(s). In order to decide the growth rate and investigate the buffer layer properties, a reference buffer layer of 3 monolayers was also grown. The obtained growth rate was then applied together with in-situ RHEED oscillations, when stopping the deposition at 3 monolayers.

2. Thick LFO thin films were grown on STO with thicknesses of 2.5, 5.0, 7.5 and $30nm$. In addition, a temperature series was grown consisting of two $7.5nm$ thick films that were grown at setpoint temperatures of 600 and $660°C$ in addition to the one grown at $540°C$. Also, LFO/LSMO heterostructures were grown on STO. The heterostructures had a $30nm$ thick LSMO layer and a 2.5, 5.0 and $7.5nm$ thick LFO layer. Also, a 30nm LSMO layer was grown as a reference.

All thin films, except for two in the temperature series, were grown at a deposition temperature of $540°C$. HF-treated substrates were used for all thin films used in the growth study because 2D growth of LSMO was not achieved on DI-treated substrates.

Optimizing Growth Parameters In the previous project LFO was grown on DI-prepared substrates with deposition setpoint temperatures of 520, 580 and $640°C$. The best results were then found at setpoint temperatures of 520 or $580°C$. As LSMO has proved to grow in stable 2D manner at lower temperatures ($500°C$) [11], the lower temperature was chosen as the main focus here. During the initialization of this work it was observed that the same setpoint temperature gave about $20°C$ lower temperature at the sample holder compared to during the project [17]. The setpoint temperature was therefore increased by $20°C$.

Initially, the LSMO thin films grown showed 3D growth at parameters previously resulting in 2D growth in the same system. Recalibration of the PLD system was therefore needed. The size of the laser focus spot on the target influence the material flux and was identified as a possible changed parameter. Good growth conditions for LSMO was obtained for growth on HF-prepared substrates, but not for DI-prepared substrates.

Throughout this work the laser has been operated at a pulse frequency of 1 Hz during deposition, one laser pulse and one second are thereby equivalents.

3.3 Reflection High-Energy Electron Diffraction

During film growth, Reflection High-Energy Electron Diffraction (RHEED) is used for in-situ monitoring of the thin film growth. RHEED is a valuable tool for in-situ monitoring of thin film growth as its low penetration depth of only a few planes makes it an ideal tool for monitoring of the thin film growth [39]. In this section, the working

principles as well as the setup will be presented before giving a review of how it may be used to identify growth modes.

3.3.1 Basic principle

A high-energy electron beam (here: 30keV) hits the substrate at a gracing incident angle. Upon hitting the substrate surface the electrons in the beam are scattered by the atoms in the first few monolayers and diffracted beams exits the the substrate. The diffracted beams then hit a phosphor screen and are detected by a CCD camera. The pattern on the phosphor screen is visible and holds information about the crystallographic surface structure and, during growth, of the growing film. It should be noted here that RHEED involves multiple scattering of the electrons and for a complete explanation dynamic scattering theory is necessary. Here, a kinematic approach is however considered sufficient in order to give a qualitative description. [40]

In figure 3.2 a schematic of a standard RHEED configuration is shown.

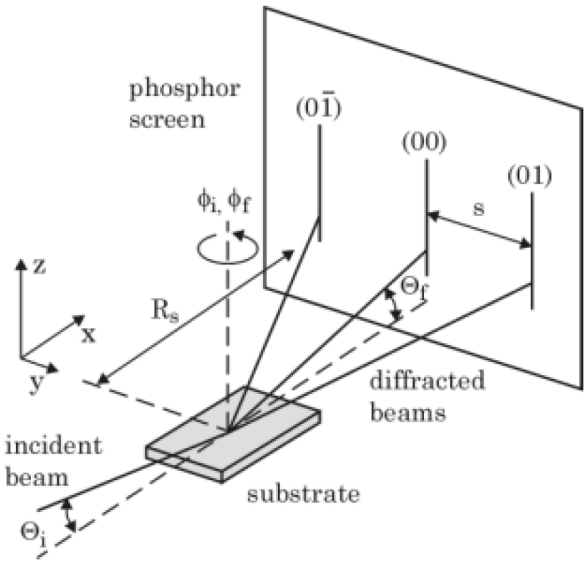

Figure 3.2: Schematic view of the RHEED geometry. θ_I (θ_F) and φ_I (φ_F) are the incident and azimuthal angles of the incident (diffracted) beam. R_S is the distance between the substrate and the phosphor screen and S the distance between the diffraction spots or streaks. Reproduced from [22]

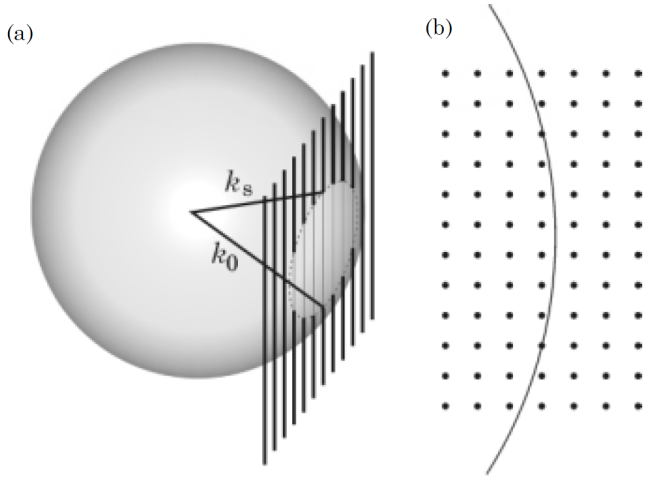

Figure 3.3: (a) Ewald sphere construction in three dimensions and (b) a section of the horizontal $z = 0$ plane. Reproduced from [22]

The diffraction pattern visible on the phosphor screen will show the reciprocal lattice of the crystal lattice. The Ewald sphere, illustrated in figure 3.3a, give a useful geometric description of the conditions of elastic scattering. A cubic crystal structure at the 2D surface is represented by a lattice of parallel rods separated by a distance $\frac{2\pi}{d}$ in in the 3D Ewald sphere, where d is the distance between atoms in the real cubic crystal lattice. By orienting the sample so that the wave vector of the incoming beam fulfills the reciprocal lattice vector G,

$$k_S - k_0 = \triangle K = G \tag{3.1}$$

where k_S and k_0 are the wave vectors of the diffracted and the incident beam, RHEED diffraction spots are produced. The diffraction spots will lie on concentric circles, known as Laue circles, formed in the intersection of the Ewald sphere and a reciprocal lattice plane, as illustrated in figure 3.3b. [22]

3.3.2 RHEED Diffraction Pattern

The RHEED diffraction pattern itself give an indication of the morphology of the surface. For a 2D surface, the diffraction spots will be sharp and lie on a concentric circle as illustrated in figure 3.4a. As the surface morphology gets rougher the diffraction spots will become more drawn out and streaks may form, illustrated in figure 3.4b. A 3D surface will be indicated by multiple spots, often arranged in a line as apposed to the arrangement on a concentric circle for 2D surfaces illustrated in figures 3.4c and 3.4d). [22]

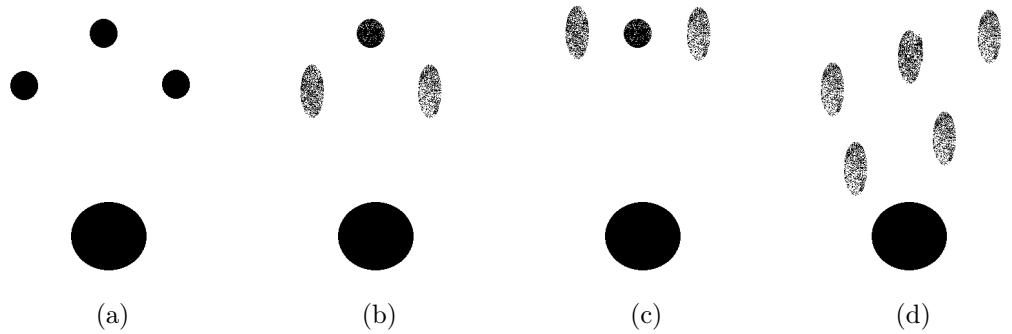

Figure 3.4: RHEED diffraction patterns expected for (a) 2D surface (substrate), (b) rougher 2D surface, (c) 3D transition surface and (d) 3D surface.

3.3.3 RHEED Intensity and Growth Modes

In section 2.2, four possible growth modes during oxide thin film growth were introduced. In this section the relationship between these growth modes and the RHEED intensity oscillations will be explained. In general the RHEED intensity fall when the surface gets rougher and rise when it gets smoother as a result of scattering.

For ideal Frank-Van der Merwe or layer-by-layer growth the RHEED intensity will fall as islands starts to form on the surface of the terraces. Then, when the islands cover $\sim 50\%$ of the terraces, the intensity will start increasing until the layer is complete. Consequently, one oscillation corresponds to the deposition of one monolayer and the deposition rate is obtained from the oscillation period. Ideally, the intensity would oscillate around a constant intensity, but in practice, islands will always start to form on top of the growing layer before the layer is completely finished and the intensity envelope will decay as a result of a general roughening.

When we have Volmer-Weber or island growth and islands form on top of islands (3D growth), the electrons will be scattered more and more as the symmetry is broken and the intensity falls. For the well defined diffraction pattern mentioned above, a perfect crystal structure is a prerequisite. As this is no longer the case in this situation the diffraction spots will start to broaden and/or change position [22].

For Stranski-Krastanov oscillations are observed until relaxation when islands starts to form and the intensity fall as for the case of Volmer-Weber growth.

With ideal step flow deposition the steps would propagate and the morphology of the surface would remain unchanged. In this situation the RHEED intensity would remain constant as no change in morphology means no change in the diffraction pattern [39]. Also, a recovery of the intensity would be observed after each pulse, as the surface diffusivity needs to be high for this growth mode.

There are a few important aspects to consider when applying RHEED to investigate initial growth. The first would be the fact that the oscillations almost always originate

from overlapping multiple layer growth instead of just one layer growth. When the conditions for formation of islands is satisfied before the growing layer is filled islands will start to nucleate on the growing layer leading to multiple open layers. As a consequence the maxima and minima will be determined by all the unfinished layers. This means that the maximum of the RHEED oscillations may not correspond to a complete layer and the minimum of the oscillations may not occur at half coverage, resulting in a phase shift of the intensity oscillations. [23]

3.3.4 In-Plane Lattice Spacing (d-spacing)

In addition to the RHEED intensity curve observed for each individual diffraction spot, the development of the distance between the diffraction spot may be used to analyze the development of the in-plane lattice spacing and the growth mode.

The distance between the diffraction spots ((10) and (-10)) is inversely proportional to the real space lattice constant and may thus be used to monitor the in-plane lattice constant (and thus relaxation) during film growth. This is done by measuring the intensity across a line (see figure 3.5a) going through the two diffraction spots and tracking the distance between the two peaks as a function of time as illustrated in figure 3.5b.

During 2D layer-by-layer growth, this in-plane lattice parameter is seen to oscillate, observed first by Massies et al [41] during $In_xGa_{1-x}/GaAs$ growth. The oscillations were explained by the lattice mismatch between the substrate and the deposited film. At complete coverage the film is fully strained and have adopted the in-plane lattice constant of the substrate, whereas at half coverage there are elastic relaxation at the island edges. The contribution from relaxation at the island edges will vary depending on island size and coverage and thus oscillate with a period of one monolayer.

Later, these oscillations have also been observed in homoepitaxy and the theory of the lattice mismatch as the source of origin is not sufficient for a complete explanation. Fuhr and Mulle [42] argue that the origin of the oscillations stem from the angular dispersion of the incident beam as islands form at the interface and the width broadening of the truncated rods. They show that the amplitude of the oscillation depends on the size of the islands, large islands leading to a larger change in d-spacing. The oscillations thus do not depend on the island edge relaxation, and may be explained by the angle dispersion at work.

The d-spacing oscillations are observed to be phase shifted by 180° compared to the RHEED intensity oscillations. The RHEED intensity is strongest for a smooth surface (full coverage) and weakest for a rough surface (half coverage). The d-spacing, on the other hand, will be largest for a rough and smallest for a smooth film. Considering Massies's theory this is explained by a higher density of relaxed island edges when the film is rough, as the island density is high, and a strained film when the film is smooth as there are no islands. From Muller's theory, half coverage would mean the point were the islands is at their largest leading to a broader diffusion spot and thus a larger d-spacing and vice-verse.

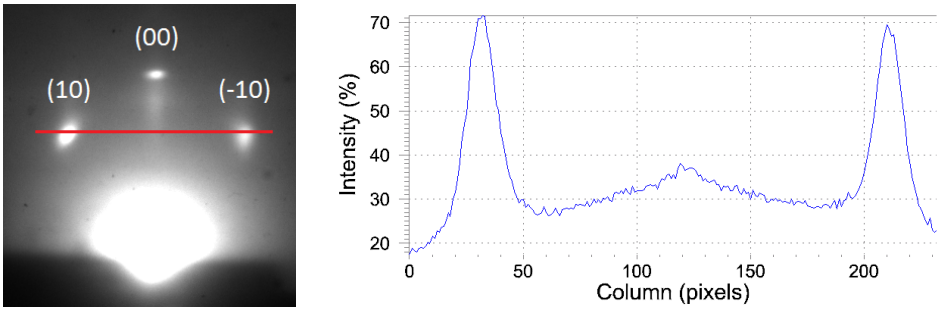

(a) (b)

Figure 3.5: (a) Illustration of the placement of the line scan. (b) Intensity line profile of substrate diffraction peaks.

In this work RHEED has been used to monitor and analyze the growth mode, d-spacing and surface roughening during growth of all thin films deposited on HF-treated substrates.

RHEED intensity oscillations have been observed during growth of most of the thin films. RHEED intensity oscillations are, for some of the films, observed exclusively on the (10) and (-10) diffraction spots and not on the (00) specular spot. When presenting, RHEED oscillations stemming from the (00) specular spot are preferred and used when possible. To distinguish between oscillations from the (00) specular spot and the (10) and (-10) diffraction spots the oscillations are assigned different colors throughout this work. Red is assigned the (00) specular spot and green the (10) and (-10) diffraction spots. Throughout this work the bulk oscillation period of RHEED intensity has been used to calculate thin film thickness.

During deposition of the thin films the distance between the diffuse spots were recorded. RHEED d-spacing curves are used to analyze growth mode and in-plane lattice constant development were available. It is done by recording a line profile on the diffraction pattern perpendicular to the streaks including the (10) spot, (-10) spot and a component of the (00) specular spot as illustrated in figure 3.5a. The inverse of this profile is then converted into the in-plane lattice spacing by calibrating the distance before deposition to the bulk lattice parameter of the substrate. The lattice spacing of the surface may be different from bulk due to reconstructions and surface effects and may be a source of error, but assumed to be small.

3.4 X-ray Diffraction

To investigate the structural quality of the thin films as well as to obtain parameters such as thickness and out-of-plane lattice constants X-Ray Diffraction (XRD) has been utilized.

XRD is a popular technique widely used in characterization of stochiometric thin films as the wavelength of the the x-ray is similar to spacing of the atoms in the crystal lattice. In x-ray characterization the x-ray hits the sample at an angle and is diffracted in a characteristic way. The diffracted beams are then recorded by a detector and maps out the reciprocal lattice of the crystal. Also, the intensity of the scattered beams depends on the atomic number of the atoms. It is thus possible to deduce the chemical nature and the arrangement of the atoms. [43]

In RHEED the electrons interact dynamically with the atoms and complicated dynamic theory is necessary for a complete analysis of material properties. In XRD the interactions are weak and a kinematic approach is, in most cases, sufficient. The waves diffract with conservation of energy and, in the case of a crystal structure, constructive interference of waves diffracted by different atoms makes up a reciprocal lattice with the same symmetry as the crystal structure. [44]

The reciprocal lattice is best viewed as the Fourier transform of the real space lattice. XRD can thus be explained theoretically considering the diffracted intensities as the Fourier transform of the real space lattice. In this work the discussion will be limited to a intuitive approach based on Bragg diffraction. Bragg's law of diffraction is given by:

$$2d \sin\theta = n\lambda \tag{3.2}$$

where d is the layer thickness, θ is the incident angle of the wave, n an integer which denotes the order of diffraction and λ the wavelength of the x-ray. Equation 3.2 is the condition for constructive interference for atomic lattice planes. [36]

The intensity of the x-rays scattered by the crystal may be expressed as the square of the scattered amplitude approximated by [34, 44]:

$$I = \frac{\sin^2(N \triangle K \alpha/2)}{\sin^2(\triangle K \alpha/2)} \tag{3.3}$$

Where N is the number of scattering planes, $\triangle K$ is the scattering vector and α is the lattice vector. For a finite value of N, the function yields a series of delta functions where the main peaks are separated by 2π and damped peaks in between are spaced by $2\pi/N$. Thus for large N, only the main peaks are visible. The fringes between the main peaks may be used to calculate the thickness of the thin film and are known as thickness fringes.

In this work a Bruker D8 discover x-ray diffractometer has been used for XRD measurements. In this instrument the sample is mounted on a goniometer that has four available angles for sample characterization (figure 3.6).

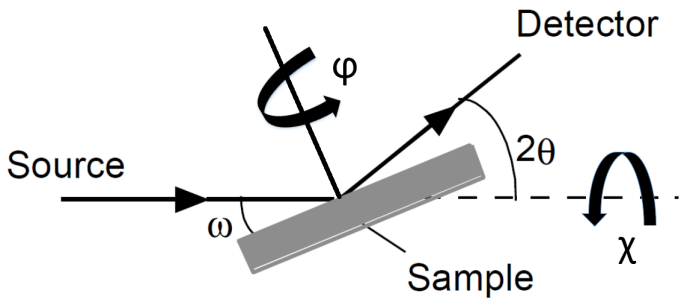

Figure 3.6: Experimental geometry of the XRD setup. ω is the angle between the incident beam and the sample surface, 2θ is the angle between the incident beam and the reflected beam, φ is the azimuthal angle and χ is the tilt angle. Adapted from [26, 36]

XRD generally refers to a range of different thin film characterization techniques, in this work the following have been used and will be explained: $\omega - 2\theta$ scans and Rocking curve measurements.

In $\omega - 2\theta$ scans only the planes parallel to the surface are measured. This is done by keeping the x-ray source fixed and rotating the sample and detector in a way that maintenance the $\omega - 2\theta$ relationship. The lattice parameter from a given Bragg reflection can be found from the the 2θ position of the Bragg peaks in the scan. As the low penetration depth of the x-rays are high compared to the thin films, a sharp substrate peak will always be visible. The peak of the thin film will be broad for thin films and gets thinner with increased thickness. Also, due to thickness fringes stemming from the finite thickness of the film (from equation 3.3), the thickness of the film may be approximately determined from the position and width of these. However, for thinner films it is difficult to get an exact measure due to the decaying value and large spacing between the thickness fringes, also the first and last layers grown will be slightly different from the rest and induce an error. [26]

Rocking curve scans, on the other hand, are done with the 2θ angle fixed and scanning the ω angle. Planes with the same (hkl) indices which are slightly different orientated are scanned to produce a rocking curve. The sharpness of the rocking curve indicates crystalline quality; the lower the full-width-of-the-half-maximum (FWHM), the higher the crystalline quality. Rocking curves can thus be used to compare crystallinity in substrate and film. [26, 36]

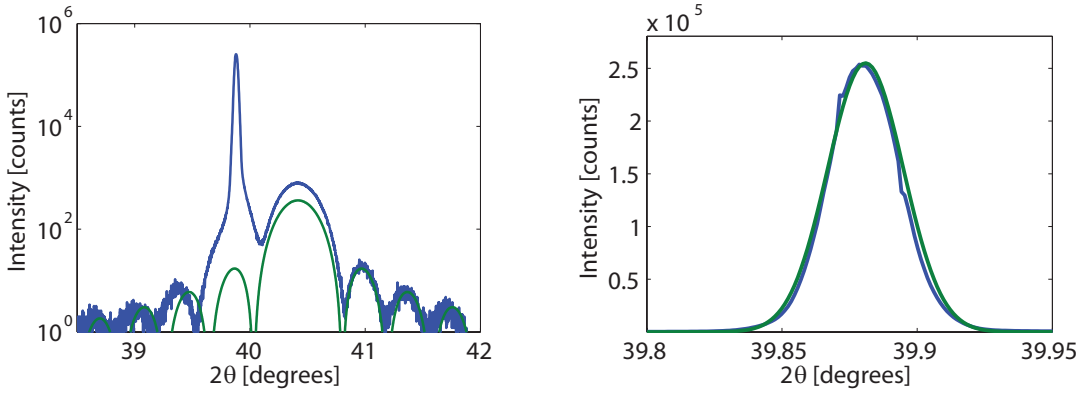

(a) (b)

Figure 3.7: Illustration of fitting of the XRD $\omega - 2\theta$ curve of a $30nm$ thick LSMO thin film to a simulated function. (a) Fitting of the $\omega - 2\theta$ curve and (b) fitting of the substrate peak to the simulated substrate peak.

In this work $\omega - 2\theta$ and rocking curve scans have been done on all samples thicker than $7nm$ grown on a HF-prepared substrate.

$\omega - 2\theta$ scans are done in order to determine the out-of-plane lattice constant of the thin film, which indicate if the thin film is strained or not. The $\omega - 2\theta$ curves are fitted to a simulation with a Matlab script as illustrated in figure 3.7. From the fitting, out-of-plane lattice constants, film thickness and growth rates are obtained. In order to achieve accurate thickness values the computer simulation of the whole XRD profile must be done. However, in this work an approximation using equation 3.3 is used. As thickness calculations become inaccurate for thin films XRD has only been done on all films thicker than $7nm$.

Rocking curve scans are done to determine the crystalline quality of the thin film.

3.5 Atomic Force Microscope

Throughout the work an atomic force microscope (AFM) in tapping mode has been used to characterize the topography of both substrate and film surface for each of the samples. The AFM is a scanning probe microscope where the forces between a tip and the surface are used to map out the topography of the surface.

In tapping mode the tip oscillates with a frequency close to its resonance frequency and is scanned over the surface. As it approaches the surface the interaction with the surface causes a change in the resonance frequency. A feedback system provided by changes in the amplitude or phase adjusts the height of the tip so that the amplitude of the oscillation is kept at a constant value. [34, 45]

The principle of the AFM has been described in more detail in previous work [17].

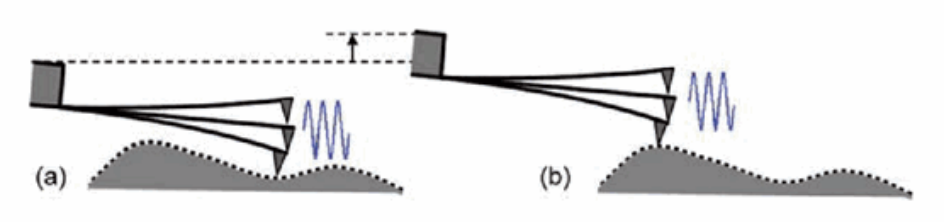

Figure 3.8: Exaggerated illustration of tapping mode AFM. A vertical displacement allows for the amplitude of the oscillation to remain constant. Reproduced from [45]

In this work Images are routinely taken after substrate preparation and then again after film deposition. The images are taken with a Veeco Nanoscope V AFM in tapping mode and are used to investigate the topography of both substrate and film. The images are leveled by three point leveling making the step-and-terrace structure visible and allowing measurements of the step-height, terrace-length and the surface roughness on each terrace. The root mean square (RMS) roughness values given in this work are an average of five RMS measurements measured on separate terraces from between two and three separate images. The area used to find each value is $100x100nm$, this value is chosen to easily obtain measurements from the short terrace films and kept constant so as to do all measurements under the same conditions.

Several definitions of a 3D surface may be found. In this study, a thin film surface is defined as a 3D surface when the RMS roughness exceeds the value of one u.c. (0.23nm).

Chapter 4

Results and Discussion

The aim of this study has been to achieve epitaxial growth and elucidate the initial growth mode of LFO on (111)-oriented STO substrates and LSMO buffer layers. In order to achieve such a goal it is important to investigate growth on both LFO and LSMO and utilize several different tools of analysis. This study consists of three main parts.

First, the results from the two methods of substrate preparation will be presented and discussed. Thereafter, initial growth of ultrathin sub-monolayer LFO on both STO and LSMO thin films will be presented. Finally, the results obtained during growth and post-deposition investigation of the continued LFO growth on STO from growth of LFO/LSMO heterostructures will be presented and discussed.

4.1 Substrate Preparation

An important parameter for epitaxial thin film growth is the substrate surface, in this section the results of the substrate preparation method will be presented along with a discussion of the results and differences between preparation methods.

4.1.1 Substrate Results

The DI-water preparation method was also applied in previous work [17], and was known to achieve a step-and-terrace surface. However, there was a large variation in both terrace-length ($54-1230nm$) and step-height ($0.12-3.60nm$) [17]. An example of a DI-etched substrate and its height profile is given in figure 4.1a and b. The step-edges were seen to be faceted with 60° and 120° edges. In some cases, triangle-terraces were observed. The triangles make up a step-and-terrace structure, but the steps are not as clearly defined, and have a larger step-height variation, compared to straight edge step-and-terrace substrates. When depositing thicker films with a high roughness, it is thus harder to identify the substrate structure. The average surface RMS roughness of the DI-prepared substrates was measured to $0.073 \pm 0.02nm$.

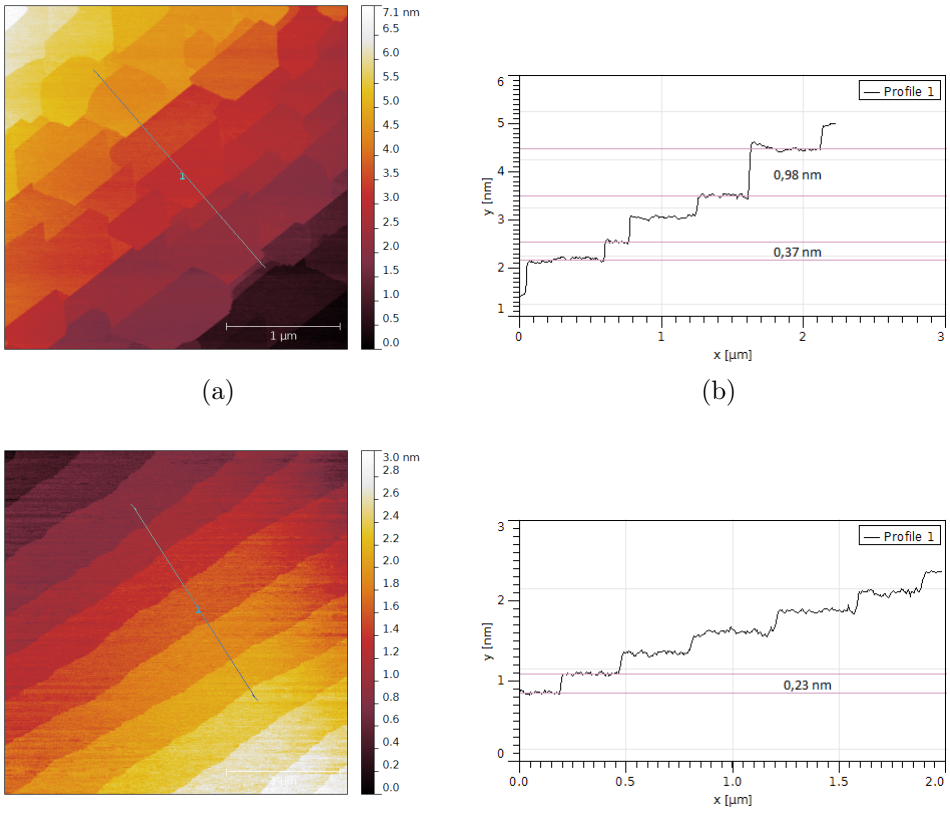

Figure 4.1: a) $3x3\mu m$ AFM image of a DI-etched (111)-oriented STO substrate. b) Height profile of a line on the substrate, showing step-height and terrace-length along the line. c) $3x3\mu m$ AFM image of a HF-etched (111)-oriented STO substrate. d) Height profile of a line on the substrate, showing step-height and terrace-length along the line.

As opposed to the substrates prepared with DI-water, HF-etched substrates all had a step-height of approximately $0.23nm \pm 0.05nm$, which corresponds to the height of one unit cell (u.c.) (see figure 4.1d). The step-edges were straight and parallel. The terrace length was observed to vary from substrate to substrate, but was generally seen to be within the same range on samples from the same substrate. The terrace lengths observed in these samples can be divided into three categories; $90-100nm$, $350-650nm$ and $\sim 1\mu m$. The average RMS roughness was here found to be $0.069 \pm 0.02nm$.

XRD measurements showed a good crystalline quality for all of HF-treated substrates. However, double peaks are observed in the rocking curve of some of the STO substrate peaks. This is attributed to twinning in the substrate. In figure 4.2a a substrate peak without twinning is shown and in figure 4.2b, a substrate peak with twinning is shown. Two of ten substrates were twinned. The FWHM obtained for the STO peak varied between 0.008° and 0.040° with a 0.019° average.

The RHEED diffraction pattern of the HF-treated substrate surface is illustrated in figure 4.3. (a) and (b) show the diffraction pattern for two different azimuth angles separated by 30°. The patterns were observed at 30° intervals, alternating between a large and a smaller distance between the diffraction spots. When changing the azimuth angle by 30° an adjustment in the tilt of the sample was also needed to focus the diffraction pattern. The relative change in distance between the two is on average 43%. The RHEED diffraction spots lie on perfect circles and are well focused.

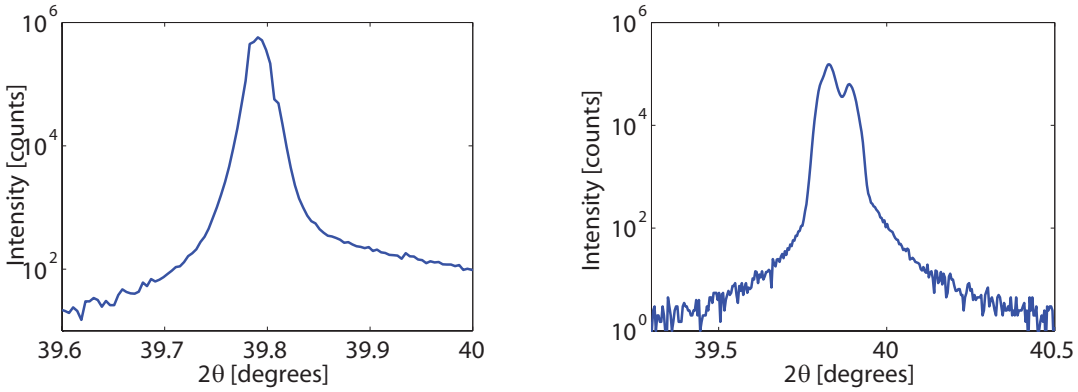

(a) (b)

Figure 4.2: Rocking curve of the substrate peak. (a) Show a sharp substrate peak and (b) show a twinned substrate peak.

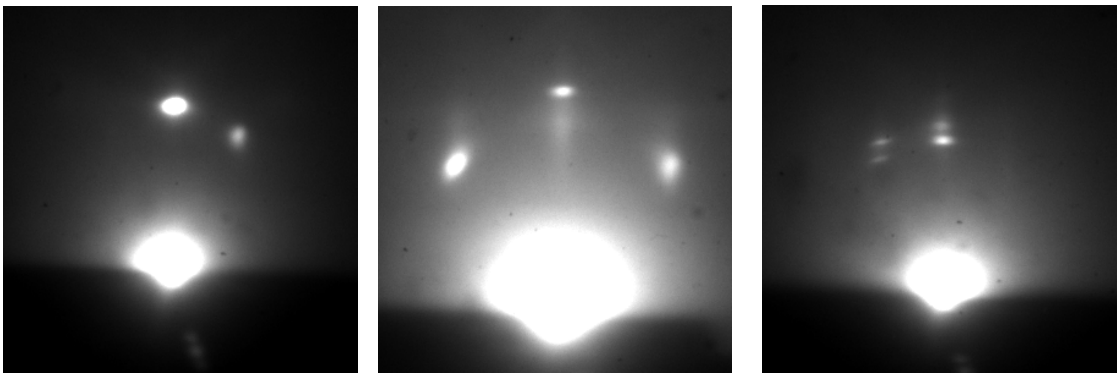

(a) (b) (c)

Figure 4.3: (a) and (b) show RHEED diffraction pattern from the substrate surface at different azimuth angles. (c) show a splitting of the RHEED specular and diffraction spot.

After optimization of the PLD system LFO was seen to initially grow in a layer-by-layer growth mode on both DI and HF prepared substrates, although it was rougher then on DI-treated in previous work [17]. LSMO grew with a 2D growth mode HF-substrates, but on DI prepared substrates it still grew with a 3D growth mode, even for thinner films. The 3D growth was mainly observed on trapeze and triangle shaped terraces as illustrated in figure 4.5a. The roughness of the trapeze shaped triangles was, on average, $\sim 2.0nm$, whereas the step-and-terrace structure around them show a RMS average value of $\sim 0.5nm$.

4.1.2 Substrate Discussion

Both substrate preparation methods yields step-and-terrace structure, but there are differences in both spread of step-height and terrace-length and step-edges.

Crystallographic Study This discussion is mainly limited to the HF-treated substrates as RHEED and XRD were done on HF-treated substrates only. The RHEED diffraction patterns in figure 4.3 from HF-treated substrates are all observed to lie on a Laue circle which indicate a 2D flat surface. Further, the fact that the diffraction pattern is observed every 30° indicate a 12-fold symmetry. This includes first and second order symmetries and equal symmetry operations, illustrated in figure 4.4. Further, the difference in distance between the diffraction spots may give an indication of which of the symmetries we are looking at, a second order symmetry (indicated by red) or a first order symmetry (indicated by green). Figure 4.3a seems to correspond to a second order symmetry since the distance between diffraction spots is small, and figure 4.3b to a first order symmetry since the distance is large. The relative difference between first and second order symmetry is theoretically calculated to 73%, which is 20% higher than the observed value. The change in tilt may be a source to the error, however, the need for a change in tilt also indicate a change in focus and may mean that we are looking at a different plane with the same type of symmetry. A change in tilt will also be a source of change in the diffraction spot distance as the optical path of the electron beam will change, explaining the difference in d-spacing between the two azimuth angles. At the (111)-oriented STO substrate the distance between planes is only $0.113nm$ [35], which means the RHEED beam's penetration depth would be sufficient. The more likely explanation is thus that we look at a different plane when changing 30° in azimuth angle, this is also further supported by the difference in visibility of the two diffraction patterns as a lower layer would mean a weaker signal.

In figure 4.3c a splitting in the specular and diffraction spot is observed, this is identified as a diffraction effect from the substrate terraces [22]. This effect has been observed mainly on substrates with short terrace length ($\sim 100nm$), and is seen to disappear when changing the azimuth angle. This confirms that it is an effect of the step-and-terrace structure, as such a contribution would fade with the turn of the substrate [22].

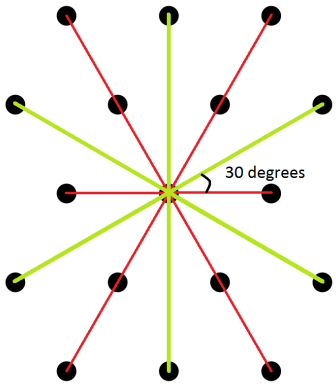

Figure 4.4: Illustration of symmetry of the (111) surface. Green corresponds t first order symmetry and green to second order symmetry.

HF versus DI The HF-etched substrates show a more stable step-and-terrace structure making the growth conditions more predictable. The fact that the substrate show a constant height of $0.23nm$ indicate a single terminated surface, and due to etch chemistry theories suggesting that Sr is removed it is believed to have a Ti^{4+} termination [28, 29]. The variation in step-heights on the DI-prepared substrates indicate a non-single termination surface which may lead to a poor interface quality. Also, the straight parallel step-edges of HF-treated substrates yields a more reproducible structure than the faceted step-edges seen on DI-treated substrates. The different angles cause a disordered surface structure which makes it difficult to identify the substrate structure through thick rough films making characterization of film morphology difficult.

When layer-by-layer growth was achieved on HF-treated substrates for both LFO and LSMO, LFO grew layer-by-layer on DI-treated as well. LSMO, however, still grew in a 3D manner as seen in figure 4.5a. 3D growth may be seen from the AFM image at trapeze shaped small terraces, whereas the growth in between has a much smoother growth mode. It looks as if the formation of small area terraces in the in the DI-treated substrates are more prone to 3D growth than large area terraces. A possible explanation may be a mixed or different termination on these terraces leading to a different diffusion and/or ES-barrier [46], but these are only speculations and would need further studies to clarify.

In conclusion it looks like the parameters yielding 2D growth on HF-prepared substrate not necessarily yield 2D growth on DI-prepared substrates. This indicate that there are differences between the two methods influencing growth conditions.

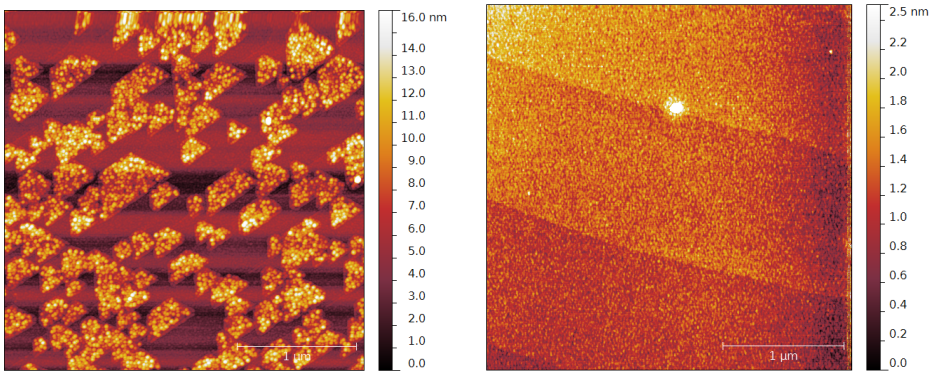

(a) (b)

Figure 4.5: $3x3\mu m$ AFM images of 2200 pulses of LSMO deposited on (111)-oriented STO substrates. a) DI-etched. b) HF-etched. Both depositions are done under the same conditions.

4.2 Initial Growth

In order to elucidate the growth modes of LFO on (111)-oriented STO it is important to understand what happens during the first couple of monolayers of growth. For this reason, sub-monolayer thick films have been synthesized to uncover how the deposited material distributes at the interface. Comparing results obtained at growth on different substrates and materials is also essential in order to identify material specific effects. Therefore a study of sub-monolayer thin films deposited on a LSMO buffer layer was done as well.

4.2.1 Ultrathin Growth of LFO on STO

As mentioned in section 3.2, two series were grown in order to obtain as much data as possible.

The first series was grown on substrates with a terrace length of $\sim 100nm \pm 10nm$, while the second series was grown on substrates with a terrace length of $\sim 390nm \pm 150nm$.

Surface Morphology AFM images taken of the substrate surface showed a step-and-terrace structure with step-height of one monolayer, the substrate structure is thus maintained.

In figure 4.6 AFM images of the first series is shown. A visual inspection of the images show that figure 4.6b is smoothest (22 laser pulses) and figure 4.6d is roughest (45 laser pulses). It seems the surface stays smooth in the three first images corresponding

to sub one monolayer thicknesses. Also in table **??**, the roughness is tabulated showing thickness and roughness. The substrate roughness is on average $0.07nm$ and the roughness is seen to increase with the number of pulses. The sample with 9 pulses deposited has a significantly higher roughness compared to all the others, this is thought to be due to contamination of the sample after growth. Disregarding this sample the roughness is seen to increase in the order of one monolayer during the growth of the first two monolayers. Considering the roughness data, it is difficult to see any clear pattern of complete versus non-complete layers, but a lower roughness around 20 pulses and an increase when approaching 45 pulses (1.5 monolayers) may be observed.

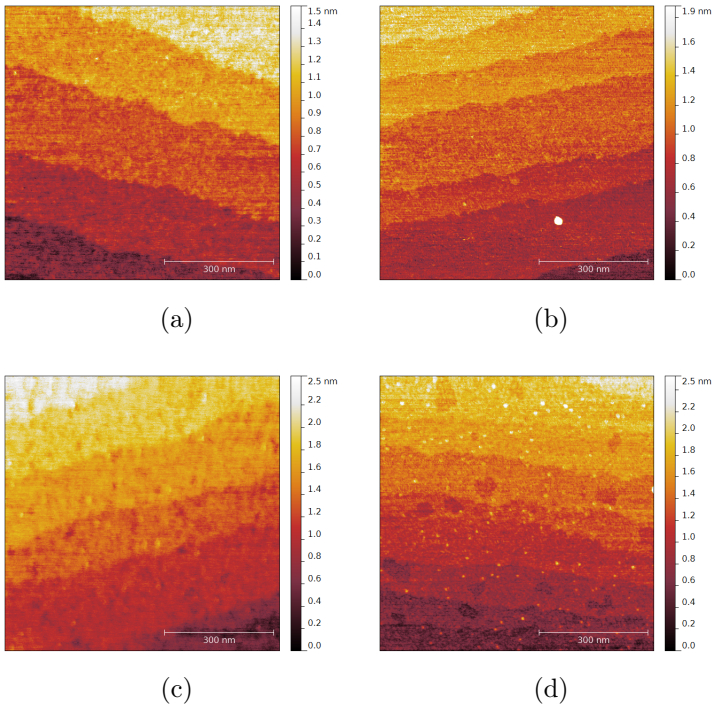

Figure 4.6: $750x750nm$ AFM images of LFO deposited on (111)-oriented STO. a) 0.5 monolayer (11 pulses). b) 0.9 monolayer (22 pulses). c) 1.2 monolayers (35 pulses). d) 1.9 monolayers (45 pulses).

Figure 4.7 show how the roughness developed with the number of deposition pulses. It may be observed that the film roughness is relatively stable over the first two monolayers. The variations are small compared to the uncertainties and it is difficult to determine completion of layers. In the first series the roughness is seen to be low after around 20 pulses, and increases at around 40 pulses, indicating full coverage at around 20 pulses and half coverage at around 40 pulses. The second series show a roughness variation in agreement with observations from RHEED intensity oscillations.

The roughness is seen to increase significantly after only 3 pulses of deposition, then decrease before a new increase at 22 pulses. It may also be observed that the different terrace length in series one and two yield little difference in roughness. Shorter terrace length seems to result in slightly smoother films, but the difference is negligible.

In figure 4.8, $250x250nm$ AFM images of some of the films from the second series are presented. The images are all cropped from $750x750nm$ images in order to investigate one terrace at a time. A color scale with large contrast is chosen in order to differentiate between layers. Black corresponds to the lowest point in the image, the height difference then corresponds to 0.23nm (one u.c.) per color change. This means that black, red, green, blue and white all correspond to different layers.

The next image corresponds to about half a monolayer deposited. In this image a much higher percentage is covered in green and almost all the holes (represented by black) in the substrate are filled. It is also possible to see formation of islands in green. However, the first layer does not have complete coverage yet.

Figure 4.8c and d both correspond to a complete layer according to RHEED oscillations, figure 4.8c to one monolayer and figure 4.8d to two monolayers. In both images it is clear that green is the dominant color, thus the coverage us high. In c, red still corresponds to the substrate and the blue areas are interpreted as islands nucleating on top of the terminating layer. In d, red now represent the first monolayer, green the second and blue the third.

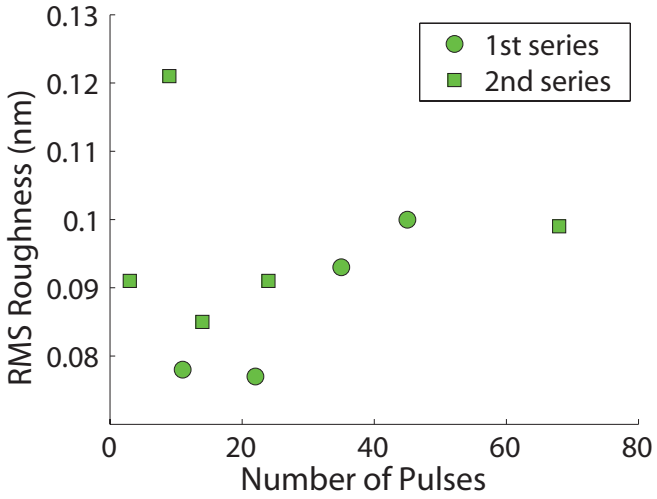

Figure 4.7: (b) RMS roughness plotted as a function of deposition pulses for LFO grown on (111)-oriented STO substrates. The circles represent the samples with shorter terrace-length while the squares represents the samples with longer terraces.

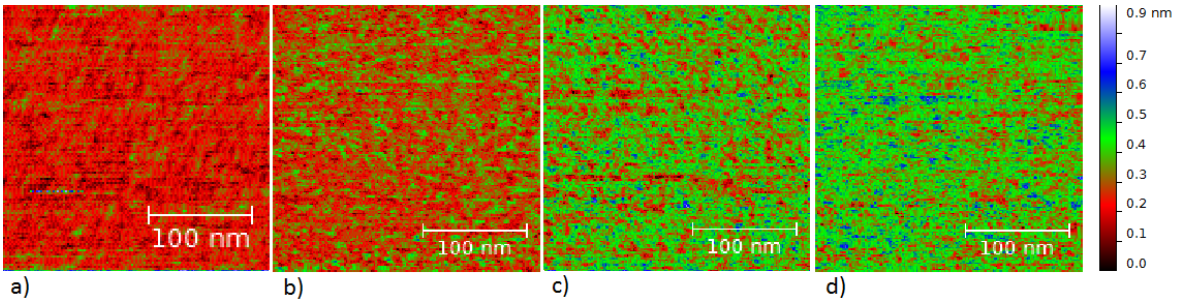

Figure 4.8: $250x250nm$ AFM images of substrate and ultra-thin films of LFO deposited on (111)-oriented STO substrates. a) Substrate surface; b) 14 pulses deposited, or ~ 0.5 monolayer; c) 24 pulses deposited, or ~ 1.0 monolayer and d) 70 pulses deposited ~ 2.0 monolayers. Colors with strong contrast have been chosen to show the different layers. Black represents the lowest point in the picture, red represents one monolayer higher, green represents two monolayers higher and blue represents three monolayer higher.

In-situ RHEED Studies The number of laser pulses before the first RHEED intensity maxima is observed to vary from sample to sample, but is seen to lie between 15 and 34 pulses (24 pulses on average). In figure 4.9 the RHEED intensity curve for the 2 monolayer thick sample is shown. It is seen that the first maxima expected to corresponding to the first monolayer occur after 24 laser pulses. The subsequent period corresponding to the deposition of the 2nd monolayer is deposited in 40 laser pulses. The average deposition rate in the second oscillation period is 45 laser pulses. Two different regimes of growth can thus be identified; the first oscillation period and following growth characterized by the 45 pulse period after the first maxima.

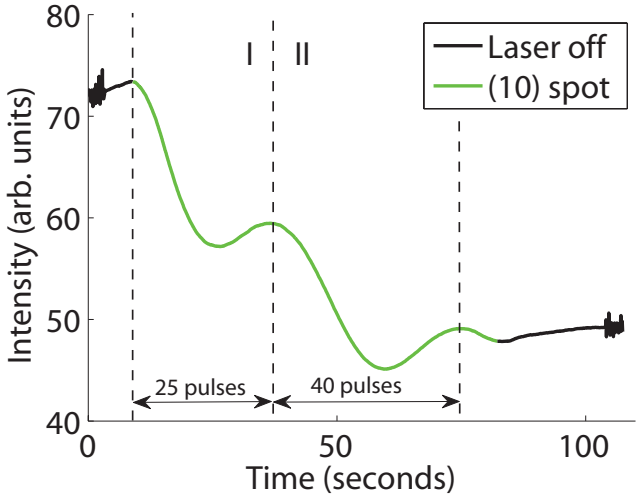

Figure 4.9: (a) RHEED intensity oscillations from the (10) diffraction spot during deposition of two monolayers of LFO on (111)-oriented STO substrate. The two growth regimes are marked by: I for the first and II for the second.

On average, the number of pulses per monolayer was thus approximately 50% lower for the first layer. In figure 4.10 it is seen that the number of pulses per unit cell has a large spread in the growth of the first unit cell, but all are lower than the number of pulses for the next layers. The colors corresponds to different films and each film is normalized around its average deposition rate after the first peak. The figure only includes films with more than two RHEED maxima, the other thin films also showed a RHEED maxima appearing after around 23 laser pulses.

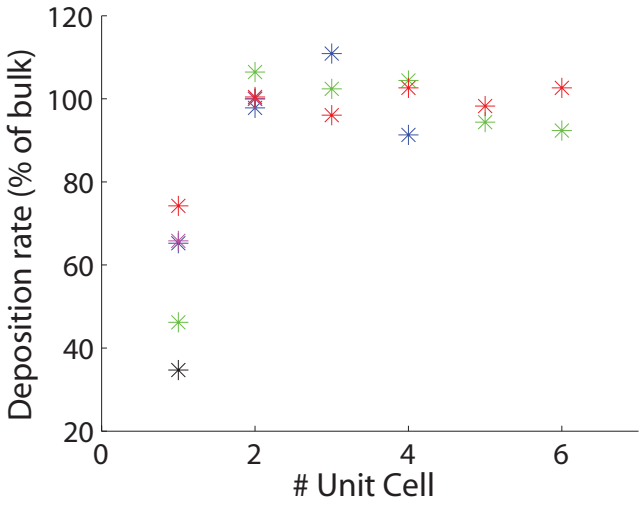

Figure 4.10: Deposition rate per unit cell during the first 6 monolayers, shown as percent of the observed bulk deposition rate for each sample. Each color represents a different sample.

When taking a closer look the RHEED intensity curve during deposition it was observed that the intensity fall for each pulse leads to no intensity recovery during first 6-7 laser pulses as seen in figure 4.11. It then show a recovery as it approaches the first RHEED intensity maxima (not shown).

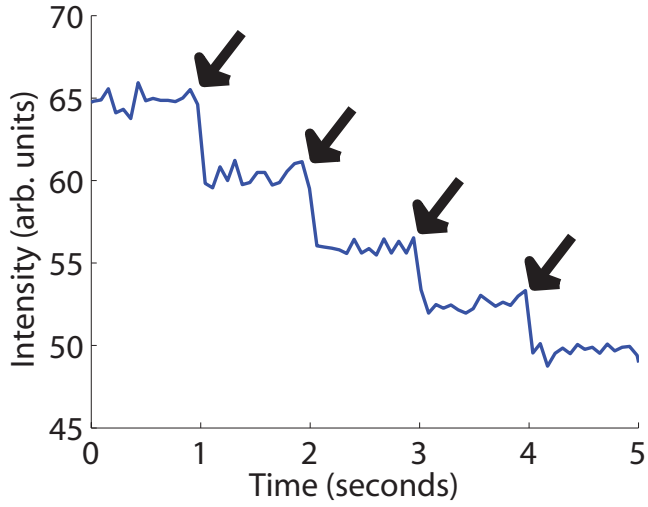

Figure 4.11: RHEED intensity at the (10) spot during deposition of the first four laser pulses of LFO on (111)-oriented STO.

In the recorded d-spacing curves of the thin films, oscillations were also observed. The oscillation curve of the d-spacing is plotted in figure 4.12 together with the RHEED oscillation from the same sample. It is clearly observed that the blue d-spacing curve is oscillating with a oscillation period equivalent to the RHEED intensity curve. The oscillation of the d-spacing curve is also approximately 180° out of phase compared to the RHEED intensity oscillations. Further, a change in the d-spacing of 0.37% from the substrate in-plane lattice constant to the observed value when the laser is turned of is also observed.

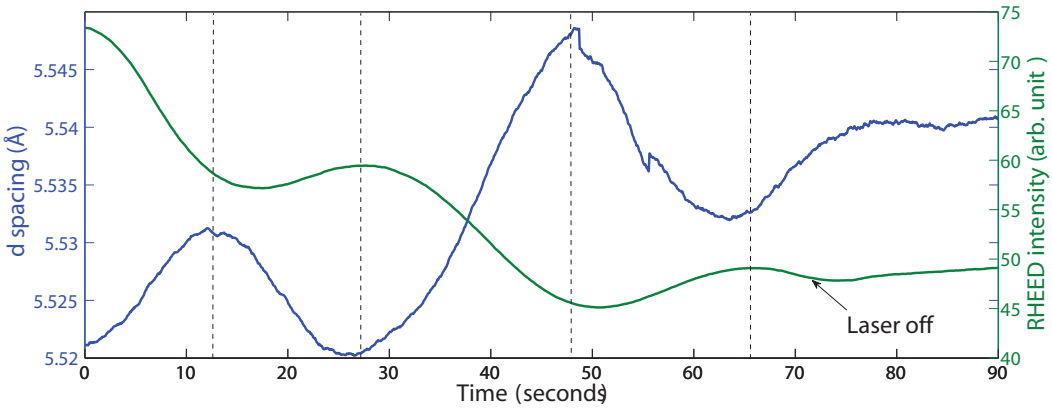

Figure 4.12: In-situ RHEED d-spacing oscillations (blue curve) and intensity oscillations (green curve) from deposition of a 2 monolayer thick LFO film on (111)-oriented STO.

4.2.1.1 Discussion

The results from initial growth investigations contain several interesting observations. First of all, observations obtained from in-situ RHEED studies indicate that the first layer is completed with half the number of pulses compared to the average deposition rate. The same observations may, to a certain degree, be observed from the AFM data. Second, oscillations observed both in RHEED intensity curves and d-spacing curves indicate a layer-by-layer growth.

Growth Mode and Morphology The observation of RHEED intensity oscillations indicate a layer-by-layer growth mode as it indicates a periodic development of the surface roughness (for a theoretical explanation see section 3.3.3). The growth rate is 45 pulses per monolayer and the first monolayer is observed after around 23 laser pulses or in half the laser pulses of the following oscillation.

Further, looking at the d-spacing curve in figure 4.12, oscillations with the same pulse period as the RHEED intensity oscillations are observed, but phase shifted approximately 180°. This is consistent with observations explained by layer-by-layer 2D island growth at (100)-oriented interfaces [41, 42, 47]. The origin and the explanation behind the oscillations and the phase shift is given in section 3.3.4.

The samples corresponding to complete layers according to RHEED oscillations seen in figure 4.8c and d show that the growing layer (green) is relatively far from completion. A phase shift in the RHEED oscillations with regards to layer completion is thus present. This may be attributed to islands starting to nucleate on top of the growing layer before the layer is complete [22].

The development of the surface roughness illustrated in figure 4.7 supports the visual observations. The low roughness values after around 10-20 laser pulses, high roughness values around 45 laser pulses and lower roughness around 69 laser pulses are in accordance with both RHEED oscillations and visual observations when accounting for a phase shift of about 10 laser pulses in the beginning. The number of samples of sub-one-monolayer thickness is higher than after one monolayer and elucidates the development during the first peak. There are fewer samples thicker than 1 monolayer and a phase shift is not as easily observed due to the "resolution" of the graph.

The growth mode is thus approximately layer-by-layer over the first two monolayers, but the early start of the second layer nucleation indicate a continued roughening and 3D development with continued growth.

The fact that the distance between the diffuse spots has decreased by 0.37% (and the in-plane d parameter thus appear to have increased), indicate that the films starts to relax from the first monolayers deposited. The value is however large, the total difference in the cubic lattice parameter between STO and LFO is 0.69% and means that the film is 50% relaxed already after two monolayers, which is not likely with such a small mismatch. A more viable explanation may originate from the observed second layer nucleation. As may be observed from figure 4.8c and d, islands starts to nucleate on top of islands. Even though there are periodical variations corresponding to deposited layers the roughness of the film increase with thickness. With a rougher film with several open layers the density of islands will increase and lead to an increase in the RHEED d-spacing envelope, as a low intensity has been shown to lead to a broader diffusion spot and an increase in the observed d-spacing [47].

According to Boschker et al [48], the roughness of the surface may be qualitatively determined by considering the development of the RHEED intensity after the initial drop. No recovery is attributed to a flat surface as the adatoms will start nucleating and form islands (increased roughness), a small recovery is attributed to a surface with a incomplete layer and a high recovery is attributed to a rougher surface were the adatoms will contribute to the filling of the layers. The development seen in figure 4.11 showing approximately no recovery thus indicate a very smooth surface. The fact that it is seen to be constant during the first few pulses may indicate that the surface stay relatively smooth during the deposition of the first pulses. In addition figure 4.8a show the substrate surface which show a clear dominance of red, with some black and

green areas. This confirms that the substrate consists of a approximately complete layer (assumed to be Ti^{4+}).

Origin of the First Growth Regime Considering figure 4.10, it is clearly seen that the average number of pulses in the first RHEED oscillation period is around half that of the following oscillation. Rijnders et al [49] observed a double oscillation period when depositing SRO on (100)-oriented STO and attributed this to a termination conversion from RuO_2 as the atomic terminating layer to SrO. A similar observation was also done during (111)-oriented growth of SRO [31]. The fact that the growth speed of the first layer here is observed to be double that of the next, initially draws to mind the possible growth of a half layer as a part of a termination conversion. However, this would mean either a mixed half layer or the deposition of twice as much of one material and non of the other.

In subsection 2.3.2 the implication of a polar substrate was discussed. Nakagawa et al [30] proposed two solutions, the first being reconstruction at the interface, but this was reported to result in immediate 3D growth [27], which is not observed here. The other alternative was a polar catastrophe solved at the interface by intermixing of atoms from the interface and the deposited material or electronic reconstruction, possible when multivalence species are present (Fe). It is thus plausible that the first layer is a mix of material from the substrate and the deposited material. This would explain that construction of the layer was done quicker and with less material then the following monolayers. The polar surface may however also be resolved by electronic reconstruction and further studies are required to make any definite conclusions.

An explanation may be that $Sr-$ vacancies in the assumed Ti^{4+}terminated substrate surface are filled, leading to a smoother surface. At the (111)-surface there are no atoms covering the Sr-atoms in the SrO^{4-}layer underneath the Ti^{4+}termination layer and Sr-atoms may thus be removed during etching. Such vacancies would then be filled leading to an overall smoother surface upon completion. The variation in the number of pulses deposited for the first maximum would then be explained by differences between the substrates. Some having more Sr-atoms removed than others. The low roughness observed after between 10-20 laser pulses and the low island coverage in figure 4.7b may indicate that the film is at its smoothest at this point after filling of vacancies.

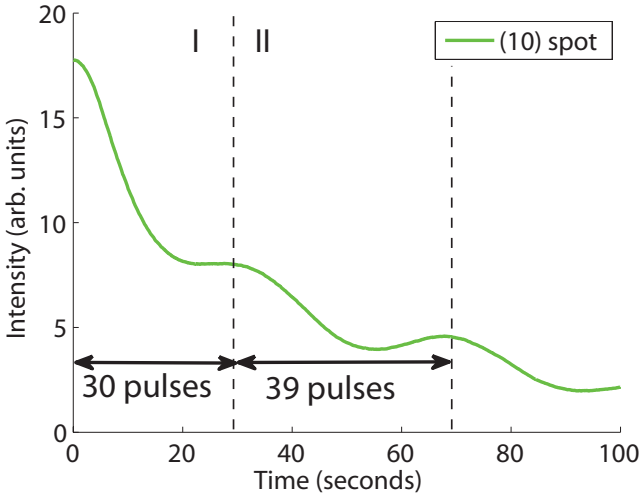

Figure 4.13: RHEED intensity oscillations from the (10) diffraction spot from a $2.5nm$ LFO thin film deposited at $580°C$ on a DI-treated substrate in previous work [17].

When taking a closer look on the RHEED pattern from the $2.5nm$ thick LFO thin film grown at $580°C$ on a DI-treated substrate in previous work [17], it is observed that the first peak appears after 30 pulses whereas the following oscillations have a period of 39 pulses (see figure 4.13). The difference in the first period between DI and HF-prepared substrate may originate from a different vacancy concentration indicating a higher concentration on DI-treated substrates. The difference in continued growth rate also indicate a different plume flux which may also influence. Most importantly it means that the two regimes are observed with DI-treated substrates also, thus it is not specific to HF-treated substrates.

In conclusion The growth starts out in a layer-by-layer growth mode with a deposition rate of 45 pulses per monolayer, but with beginning second layer nucleation. The first monolayer is grown in approximately half the number of pulses and is attributed to filling of $Sr-$ vacancies at the interface leading to a mixed layer.

4.2.2 Ultrathin Growth of LFO on LSMO

Also, a study of sub-monolayer thin films of LFO grown on a 3 monolayer thick buffer layer of LSMO was done during this work. This was done in order to investigate differences between initial growth directly on a (111)-oriented substrate and a (111)-oriented buffer layer.

In-situ RHEED Studies The three monolayer thick LSMO buffer layer grown as a reference had a roughness of $0.08nm$ and a constant deposition rate of about 15-19

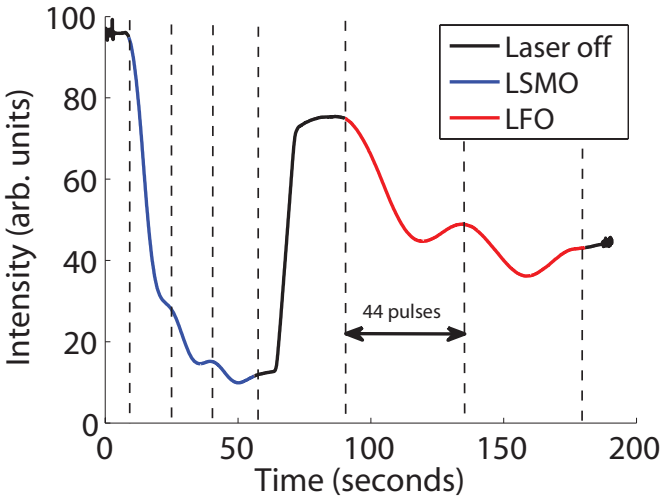

Figure 4.14: RHEED intensity oscillations of the specular (00) spot during deposition of a 3 monolayer thick LSMO buffer layer and a 2 monolayer thick LFO thin film. The black line represents the time when the laser is off, the blue line the deposition of LSMO and the red line the deposition of LFO.

laser pulses per monolayer over the first three monolayers. The two growth regimes characterized by a difference in RHEED oscillation period observed in LFO growth on (111)-oriented STO, is thus not observed for LSMO on STO.

In figure 4.14 the oscillations of both the LSMO buffer layer and the LFO thin film are clearly observed across the interface and the deposition rate may be calculated accordingly. For the LFO thin film, the first maximum is observed after about 45 pulses and the second maximum after about 90 pulses. This indicates a constant growth rate from the first monolayer of 45 pulses per monolayer.

D-spacing curves were not obtained during growth of these samples due to a to low intensity on the diffraction spots.

Surface Roughness As may be seen from figure 4.15, the roughness of the respective LFO thin films show a periodic development in phase with the RHEED oscillations. The thin films corresponding to a half and one and a half monolayer of LFO show a larger roughness than the samples corresponding to one and two monolayers. It should be noted that we only have four samples and the variations of the roughness is relatively small, so this may be a coincident. The four films grown are presented in figure 4.16 and in table 4.1. The RMS roughness is seen to be in the same magnitude as on STO even though the buffer layer is rougher than the STO substrate.

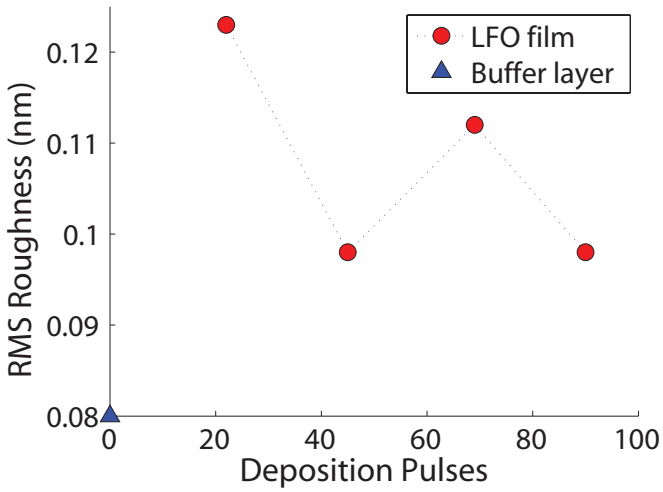

Figure 4.15: RMS roughness plotted as a function of deposition pulses for LFO grown on LSMO buffer layer. The red circles represent the roughness of the LFO samples and the blue triangle represents the roughness of a LSMO 3 monolayer thick reference layer.

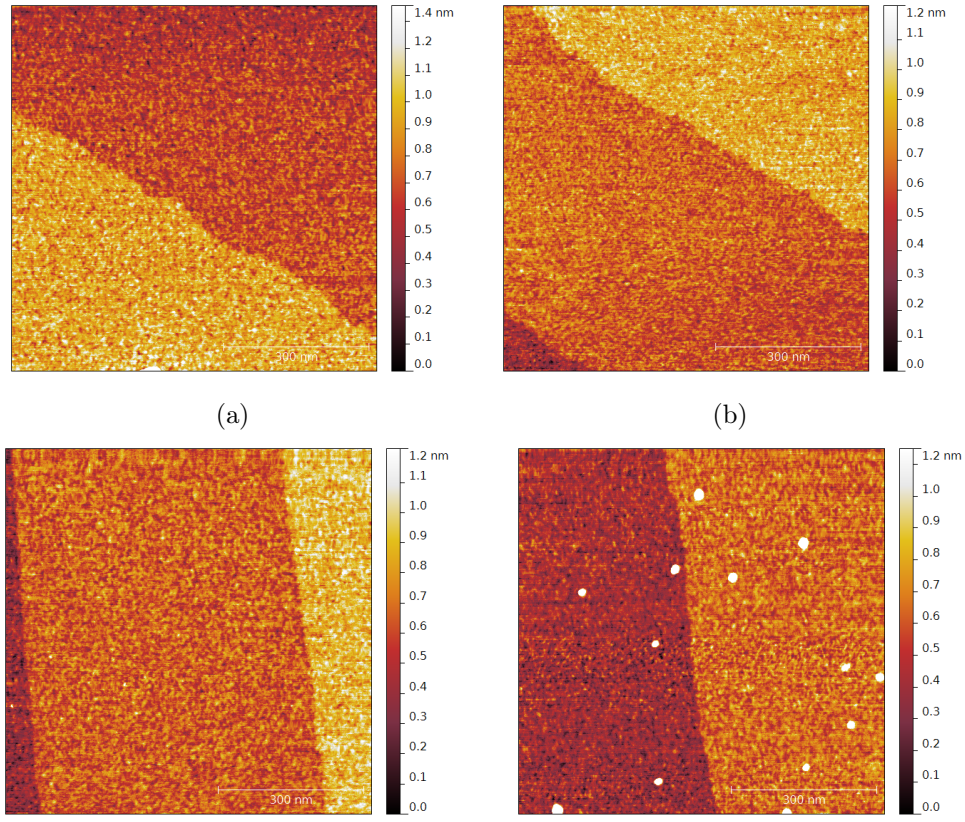

Figure 4.16: 0.75x0.75 um AFM images of LFO grown on 3 monolayer thick LSMO buffer layers. (a) 0.5 monolayer (12 pulses), (b) 1 monolayer (45 pulses), (c) 1.5 monolayers (69 pulses) and (d) 2 monolayers (90 pulses).

Sample	Material	# Pulses	Thickness [u.c.]	RMS Roughness [nm]
p30505	LSMO	50	3.0	0.080
p30511	LFO/LSMO	22/45	0.5/3.0	0.123
p30509	LFO/LSMO	45/45	1.0/3.0	0.098
p30508	LFO/LSMO	69/45	1.5/3.0	0.112
p30507	LFO/LSMO	90/45	2.0/3.0	0.098

Table 4.1: Overview of LFO thin films grown on a 3 u.c. LSMO buffer layer.

4.2.2.1 Discussion

The results from growth of LFO on LSMO buffer layers contains some interesting observations. Especially, the constant growth rate over the first two monolayers and the correlation between roughness and RHEED oscillations are interesting.

In-situ RHEED Studies Since the there was only one growth regime observed when growing LSMO on STO it might indicate that the two growth regimes characterized by a difference in the RHEED period is specific for the LFO/STO interface, and not a general effect for (111)-oriented TMO growth on STO. However, the deposition period is shorter and comparable to the first oscillation observed on LFO and may keep us from observing the difference. A smaller number of laser pulses per monolayer also leads to a lower resolution for observation, making it more difficult to identify. Further, the RHEED oscillations observed during LFO growth on the LSMO buffer layer also show a constant deposition rate of around 45 pulses per monolayer from the first monolayer. This is another indication that the effect observed on LFO/STO interface growth is specific to the STO substrate and not specific to LFO growth on (111)-oriented substrates. The theory of $Sr-$ vacancies is therefore still plausible.

Growth Mode The variations in the film roughness (figure 4.15) seen in connection with the RHEED oscillations (figure 4.14) show an interesting coincidence. Where the RHEED oscillations predicts half coverage the roughness is high, and where the RHEED oscillations predict full coverage it is low. This is in accordance with half grown and complete monolayers respectively, and indicates that the RHEED oscillation is in phase with the development on the surface roughness. As the variations are small and the uncertainties comparable, this may be a random coincident. However, it may also be a confirmation of a layer-by-layer growth with a 45 pulse period.

In figure 4.17, AFM images of terraces of 0.5, 1.0, 1.5 and 2.0 monolayer thick films are shown. The different colors represents different monolayers. Considering figure 4.17a and c it is seen that the distribution in colors is higher than in figure 4.17b and

d. This further confirms what has been indicated in both RHEED oscillations and RMS roughness measurements, that the coverage is lowest after 22 and 67 pulses and highest after 45 and 90 pulses. The presence of up to four colors in the images also indicates that several layers are open at the same time. For example in figure 4.17b and d green is assumed to be the "terminated" layer, while red represents the underlying layer and blue represents a new layer nucleating on the terminating layer. The phase shift observed at LFO/STO is therefore also likely to be present here.

The growth mode across these first monolayers is thus approximately layer-by-layer, but with several open layers which with thickness may lead to a 3D surface.

The surface roughness is also comparable to the roughness of the LFO thin films grown directly on the STO substrate. Since the films are grown on a buffer layer, the roughness might increase as a consequence of the buffer layer not being terminated at exactly full coverage. Considering this and observing that the relative change in roughness is unchanged over the two fist layers, it may be argued that LFO grow smoother on a LSMO buffer layer. This may indicate a prolonged layer-by-layer growth of LFO on LSMO compared to on STO. In section 2.3.2 the screening of the polar interface by metallic SRO leading to a smoother growth of BFO and SFO observed by Blok and Chang [27, 32] is discussed. LSMO is half metallic and might serve to screen the polar surface leading to a smoother growth. However, the data collected in this work is very limited and only an indication, only showing the first two monolayers of LFO growth, and further studies are needed in order to make a conclusion.

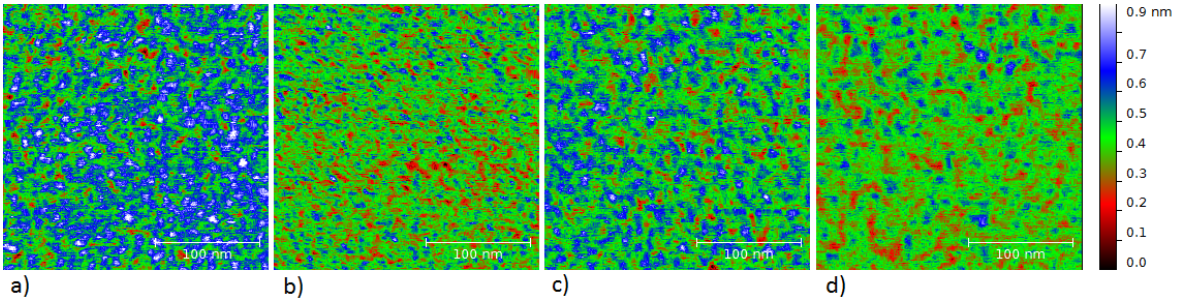

Figure 4.17: $250x250nm$ AFM images of (a) 0.5, (b) 1.0, (c) 1.5 and (d) 2.0 monolayers of LFO grown on a 3 monolayer thick LSMO buffer layer. The images are cropped from $500x500nm$ images and show the surface at individual terraces. The colors represents different heights in the surface topography and corresponds to the values seen in the ruler.

In Conclusion The double deposition rate observed at the interface between LFO and STO is not observed at the LFO/LSMO buffer layer interface, but may still be there. This indicates that the effect may be specific to the LFO/STO interface. Moreover, the phenomenon is not observed for any of the LSMO/STO interfaces grown, indicating

that it is a specific effect for LFO at the substrate surface. The oscillation period is however shorter and a vacancy filling may be disguised in the first oscillation. If it is a $Sr-$ vacancy filling it would be expected to appear in LSMO as well.

The slightly smoother development of the LFO thin film on LSMO may also indicate that LSMO screens the polar surface leading to a higher degree of layer-by-layer growth and a possibly a prolonged growth mode.

4.3 Thick Growth

The initial growth is important in order to understand and investigate the growth mode and effects at the interface, but the continued growth is also important as most applications require thicker films. A series of thicker LFO thin films on STO was therefore grown in order to investigate the continued growth. Also, for application, synthesis of LFO/LSMO heterostructures are interesting. LFO/LSMO heterostructures are therefore grown in order to gain knowledge of LFO growth on thicker LSMO thin films.

4.3.1 LFO on STO

In this section films of thicknesses 2.5, 5.0, 7.5 and $30nm$ deposited at $540°C$, and a temperature series of $7.5nm$ thick films at 540, 600 and $660°C$ will be presented.

In-situ RHEED Studies RHEED intensity oscillations were observed during some of the depositions. At a deposition setpoint temperature of $540°C$, RHEED oscillations were observed on the diffraction (10) spots only, on two films. On a third film ($30nm$), RHEED oscillations were observed on the (00) specular spot. The intensity fell exponentially before leveling out and continuing with a slightly falling intensity, for all the diffraction spots showing oscillations. The oscillations were seen to be damped out at around 400-500 laser pulses of deposition. The RHEED oscillations observed on the (10) spots show a deposition rate of 44-48 pulses per monolayer, whereas the oscillation observed on the (00) specular spot (for a different sample) show a constant growth rate of 44 pulses per monolayer.

Also during thicker growth, oscillations in the d-spacing were observed. The oscillation period corresponds to the oscillation period of the RHEED intensity for the spots and is phase shifted approximately 180°. In addition to the oscillations a large gradual increase in the distance is observed. The shift is larger than what would be expected for a relaxation from the STO parameter ($5.52\mathring{A}$) to the LFO parameter ($5.56\mathring{A}$).

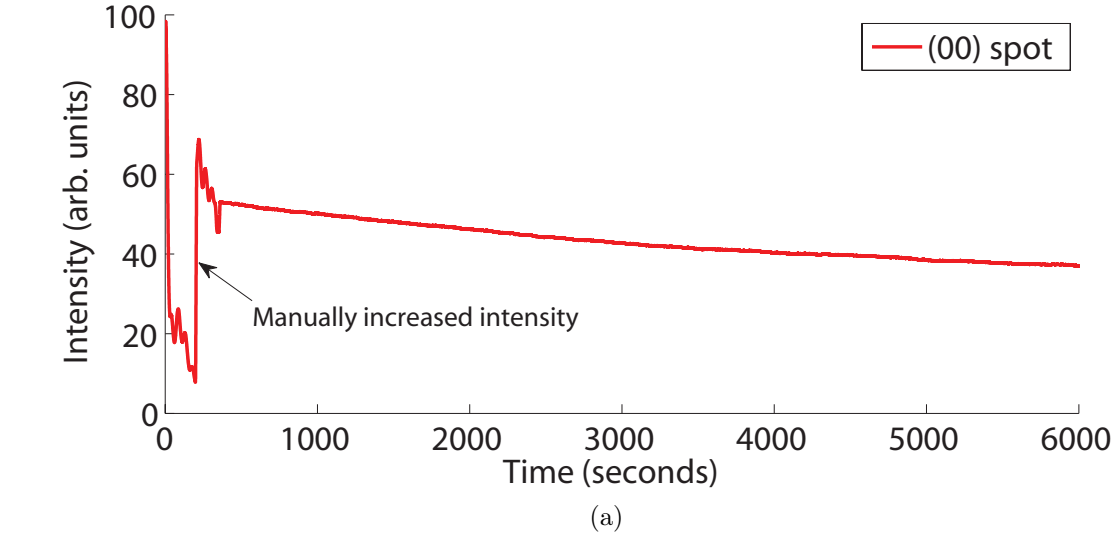

(a)

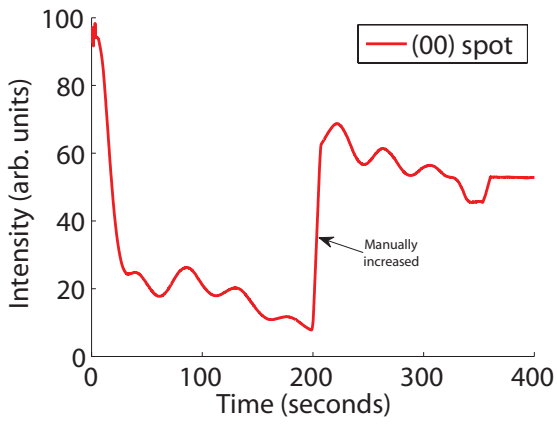

(b)

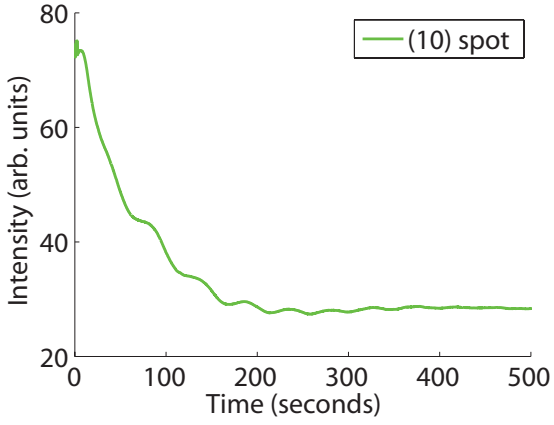

(c)

Figure 4.18: RHEED intensity oscillations from LFO deposited on (111)-oriented STO at a setpoint temperature of $540°C$ are shown here. a) RHEED oscillations from deposition of 30nm LFO as recorded from the (00) spot. b) A cut out from image a), showing the first 400 seconds of deposition. c) RHEED oscillations from deposition of LFO recorded at the (10) diffraction spot from a different sample.

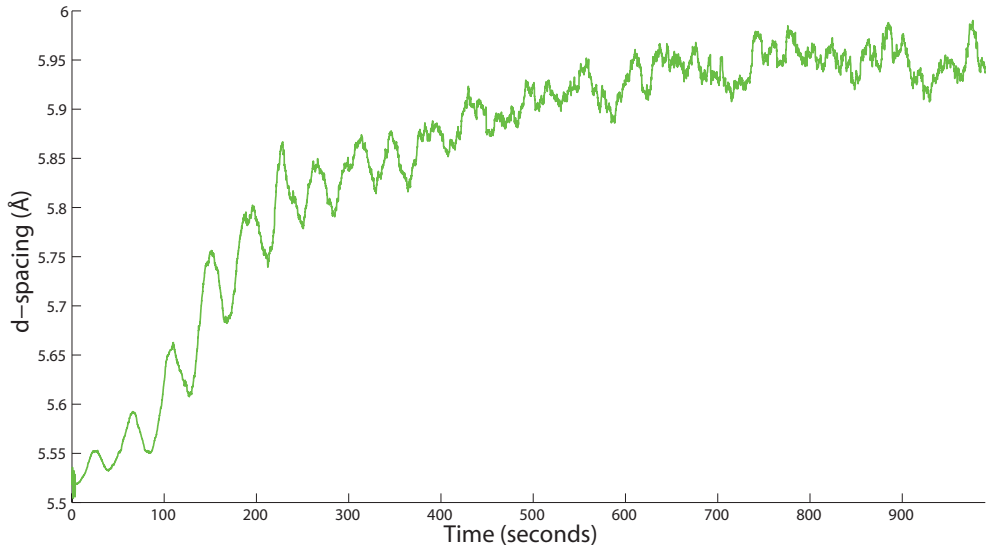

Figure 4.19: Development of the distance between the (10) and (-10) RHEED diffraction spot for the $5nm$ thick LFO thin film (sample p30420).

In figure **??**, the diffraction patterns after growth from the 2.5 (b), 5.0 (c) and $7.5nm$ (d) thick LFO thin films are shown together with a RHEED pattern from the substrate (a). The spots are drawn out for the $2.5nm$ thin film, they appear on a line for the $5nm$ thick film and several spread spots appear for the RHEED pattern from the $7.5nm$ thick film.

Surface Roughness In figure 4.20, AFM images of LFO thin films with thicknesses between 2.5 and $30nm$ are shown. By visual inspection it is seen that the structure of the substrate has been adopted by the thin film. Looking at figure 4.20a the step-and-terrace structure is clearly visible, though a roughening has happened, the same holds for the 5.0 and $7.5nm$ thick films. However, for the $30nm$ thick LFO thin film it is much harder to recognize the surface structure, indicating a 3D surface. The roughness of each film is given in table 4.2. From the AFM images in figure 4.20, an increase in surface roughness is also seen as the film gets thicker.

In figure 4.21, the RMS roughness for all the LFO films grown are plotted as a function of the film thickness with a logarithmic axis. The roughness seems to be increasing rapidly during the first $7-8nm$, and then increases at a lower rate. Between 2.5 and $7.5nm$, the increase in roughness is linear, just like for growth on DI-substrates in previous work [17]. However, the roughness is seen to be much higher, already at $0.207nm$ for the $2.5nm$ thick film.

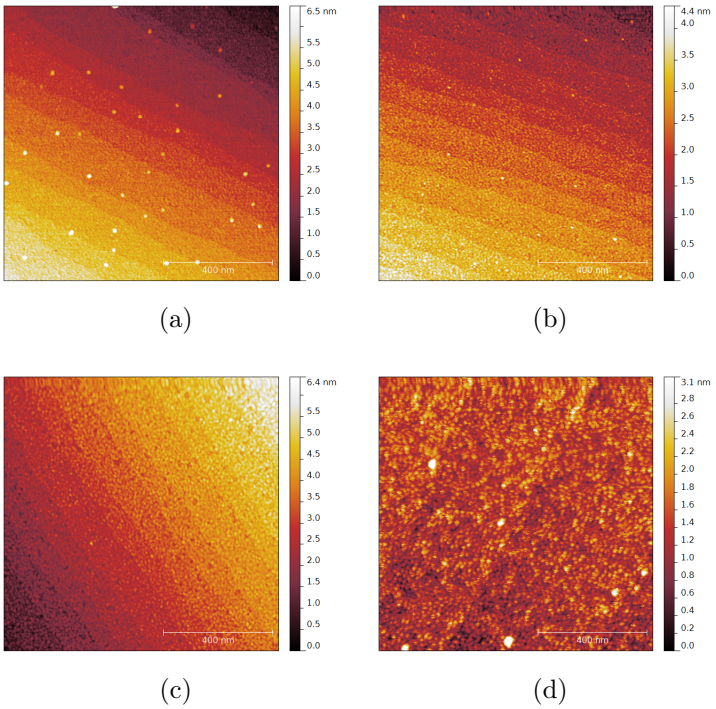

Figure 4.20: $1x1\mu m$ AFM images of LFO thin film grown on (111)-oriented STO substrates at $540°C$. a) 500 pulses deposited, corresponding to 2.5nm. b) 1000 pulses deposited, corresponding to 5.0nm. c) 1500 pulses deposited, corresponding to 7.5nm. d) 6000 pulses deposited, corresponding to 30nm.

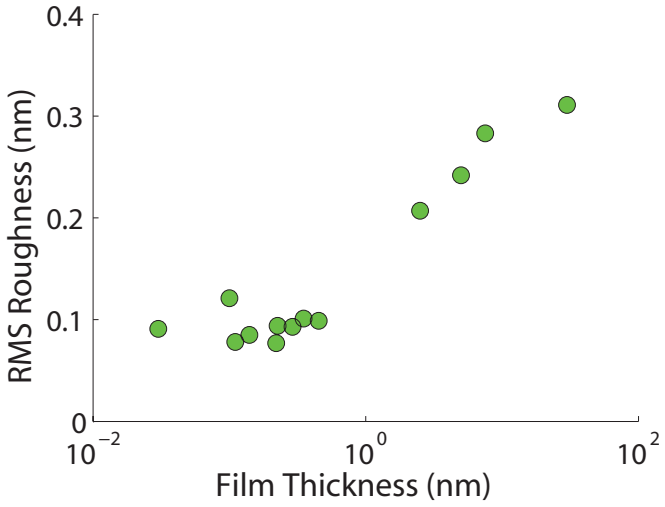

Figure 4.21: RMS roughness for LFO thin films grown on (111)-oriented substrates as a function of thin films. The thickness is plotted with a logarithmic scale.

Temperature In order to identify the growth mode at the interface, temperature can be used as a parameter.

To examine the influence of the HF-prepared substrate compared to the DI-prepared, samples with setpoint temperatures of 540, 600 and 660°C were grown. The resulting films are shown by AFM images in figure 4.22 and the RMS roughness for each film is presented in table 4.2. The thin film surface is seen to get rougher with increased temperature both from visual inspection of the AFM images and RMS roughness measurements done on the images. The thin film grown at a setpoint temperature of 660°C show a rough surface with holes, the surface structure of the substrate is also not easily observed (see figure 4.22c).

The in-situ RHEED intensity curves acquired for these films did not show consistent oscillations and development as for deposition at 540°C, but some oscillations were observed. During growth with 600°C the first RHEED intensity maxima occurred after 12 pulses, and the two following periods were 48 and 51 pulses at the (00) specular spot. For the 660°C deposition, RHEED intensity oscillations were observed on the (10) diffraction spot between 300 and 500 pulses with an average period of 59 pulses.

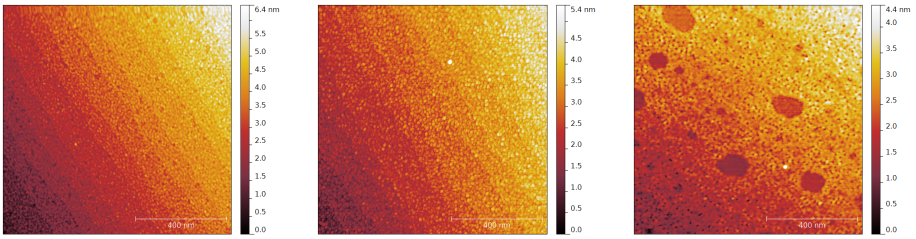

(a) (b) (c)

Figure 4.22: 1x1 um AFM images of LFO thin film deposited on (111)-oriented STO with a setpoint temperature of: a) 540°C, b) 600°C and c) 660°C.

Crystalline Characterization The structural quality of the thin films are investigated by XRD and show a high structural quality for all thin films. Rocking curves were extracted from the 7.5nm thin films and the 30nm thick film and show an average FWHM of the substrate STO peak of 0.023° (see table 4.2). For the thin films grown at 540°C the LFO FWHM was 0.056° for the 7.5nm film and 0.045° for the 30nm film. This is higher than the others, but attributed to a twinning in the substrate, observed in the substrate peak. For the LFO thin films deposited at higher temperatures the FWHM is 0.039° for the one deposited at 600°C and 0.020° for the one grown at 660°C (with comparable substrate).

The out of plain lattice constant of LFO found from a $\omega - 2\theta$ scan of the 30nm thick film is found to be $d_{110} = 0.228nm$. This is 1.1% higher than the cubic lattice parameter of the STO substrate and 0.44% higher than the LFO pseudo-cubic lattice parameter. The calculated thickness is 20.5nm whereas the thickness calculated from the RHEED oscillation period is 30nm. The growth rate is in the same way calculated to 2.1$\mathring{A}$ per minute from XRD and 3.1$\mathring{A}$ per minute from RHEED oscillations. As may be observed in figure 4.23, the thickness fringes are not easily identified and an error margin connected to the simulated fitting curve must also be taken into account.

Sample	T_s[°C]	Thickness [nm]	RMS roughness [nm]	FWHM (substrate) [°]
p30421	540	2.5	0.207	N/A
p30420	540	5.0	0.242	N/A
p30419	540	7.5	0.283	0.056 (0.040)
p30518	540	30	0.311	0.045 (0.029)
p30521	600	7.5	0.326	0.039 (0.011)
p30522	660	7.5	0.336	0.020 (0.010)

Table 4.2: Overview of some properties of thin films grown on (111)-oriented STO.

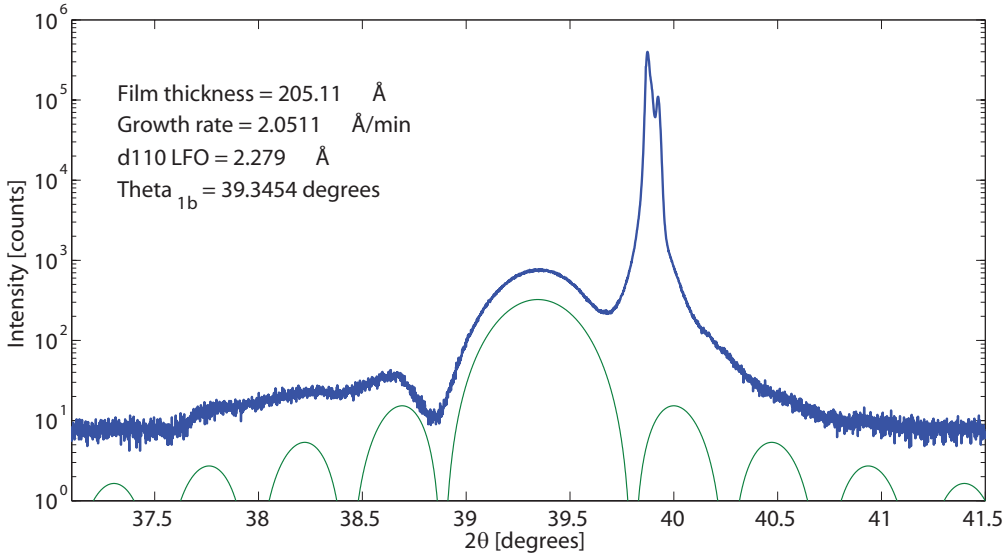

Figure 4.23: Measured $\omega - 2\theta$ scan of the 30nm thick LFO thin film grown on (111)-oriented STO. The sharp peak is the STO (111) substrate peak and the broader peak left of it is the LFO (111) peak.

4.3.1.1 Discussion

In previous work, LFO was grown at three different thicknesses (2.5, 5.0 and 7.5nm) and temperatures (520, 580 and 640°C) on DI-etched substrates. In this work, LFO thin films with the same characteristics were grown in order to compare the results from DI and HF prepared substrates. One of the most interesting observations of this section is the observed transition from a 2D to a 3D surface at around 5nm, also the roughening with increased temperature is interesting when compared to results on DI-prepared substrates in previous work [17].

Growth Mode Both the RHEED intensity oscillations and the 180° phase shifted d-spacing oscillations observed over the first 400-500 laser pulses indicate a 2D island layer-by-layer growth. Also, considering that the RMS roughness of the 2.5nm thick thin film is lower than a u.c., a 2D surface in this interval is further confirmed. However, as the amplitude of the RHEED intensity oscillations are damped out and the underlying trend of the d-spacing is increasing, it seems that the initial 2D island layer-by-layer growth starts involving more layers and transition into a 3D island growth mode after around 500 pulses. From the diffraction pattern in figure **??** and the RMS roughness in table 4.2 the surface of the 5.0nm thick film may be identified as 3D, further confirming the growth mode transition. As discussed in section 4.2.1.1, nucleation on the growing layer is observed already during the first two monolayers, which support a early transition

into 3D growth. At 7.5nm the film clearly has a 3D surface as the RMS roughness value is higher than one u.c. and the diffraction pattern show multiple spots (see figure **??**). A complete transition into 3D growth is thus confirmed. The linear increase observed between 2.5 and 7.5nm along with figure 4.8 in section 4.2.1 showing early second layer nucleation, also indicate that the multiple layer nucleation is constant leading to an increase of island density.

The rate of roughening seems to slow down between 7.5 and 30nm and a new growth mode may emerge upon further studies of thicker films.

Strain Looking at figure 4.19, the in-plane lattice parameter is seen to increase by 7.8%, overshooting the bulk LFO value by 0.39$\mathring{A}$. Such an increase would mean a complete relaxation and some unexplained increase, which is unlikely. From the $\omega - 2\theta$ scan an out-of-plane lattice constant of 2.28$\mathring{A}$ is observed for the 30nm thick film. This would mean an increase of 0.44% compared to bulk LFO values (2.27$\mathring{A}$) and indicate a strained film as discussed in section 2.2.7, this is also in accordance with out-of-plain elongation for (100)-oriented strained growth of LFO on STO [37]. It thus looks like the thin film is strained and the large change in the d-spacing must have another origin. Further, the small difference between substrate and thin film FWHM observed on rocking curve measurements confirms a good crystalline quality for all the films. The thickness fringes in figure 4.23 are not as clearly defined as one would expect for a high quality film of this thickness, the reason is assumed to be the twinned substrate (as may be observed in the substrate peak).

The large increase in the measured d-spacing may be explained by a combination of origins. The origin of the oscillations was identified as the variations in island densities and island size [42]. As the film gets rougher and grow into a 3D island growth mode, more and more open layers contribute to the angular dispersion of the diffracted beam. The oscillations were accounted for by a periodic development, where islands form, grow and are evolved into a new layer. The general increase in roughness is not periodic, it also leads to a islands forming on islands, like a wedding cake. there will thus be islands of different sizes contributing to the dispersion of the RHEED beam.

A related contribution, especially for the thicker films may stem from the fact that the intensity of the diffraction spots falls of as the roughness increase and the detection of the tops becomes more difficult and less accurate (see figure 4.24). As the peaks vanish completely they become indistinguishable and the tracking function will search for a higher peak moving towards the center which appear as an increase of d-spacing in real space.

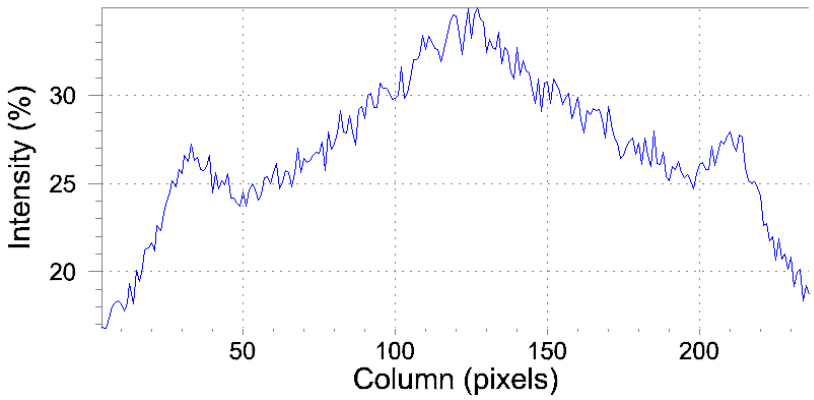

Figure 4.24: The line profile from the d-spacing between diffraction spots during deposition of LFO on (111)-oriented STO. The line profile is taken during deposition and demonstrate that the peaks become more diffuse and difficult to detect. Upon further roughening they vanish completely.

Temperature As the roughness is seen to increase with temperature, the applied temperature ($540°C$) seems to yield the best results. At $600°C$ the roughness has increased, but at $660°C$ the surface has started to break up and become unstable, leading to holes with diameters from 20 to $250nm$ in the surface. An increased adatom mobility may thus work to destabilize the surface as was also the case for LSMO [11]. This may be related to the 3D growth observed at $800°C$ for growth of SFO, attributed to low oxidation powers leading to unstable conditions for Fe [32]. The fact that the first RHEED maxima is observed after only 12 pulses may be a coincidence due to the poor RHEED data, but it may also be explained by an increased adatom mobility leading to a faster filling of vacancies. Further, a slightly lower deposition rate for $600°C$ and an even lower deposition rate at $660°C$ is observed from RHEED oscillations indicating a decline in the growth rate with increased temperature. The lack of observed oscillations may also explain the increased roughness by indicating a 3D island growth mode, if not from the first layer at least from an earlier point than at $540°C$.

HF versus DI Prepared Substrates The transition from a 2D to a 3D thin film surface was not observed until between 5.0 and $7.5nm$ for growth on DI-substrates compared to between 2.5 and $5.0nm$ for HF-treated substrates [17]. The $2.5nm$ thick film grown on a DI-prepared substrate in previous work had a roughness of $0.10nm$, while the corresponding thin film in this work had an RMS roughness of $0.21nm$ [17]. From figure 4.13 it may also be seen that the thin films in previous work [17] were grown with a higher deposition rate.

The observation is thus that LFO grow smoother under similar conditions on DI-prepared substrates as compared to HF-prepared substrates. The difference in rough-

ness may, however, originate from differences in the plume flux, as the PLD system has been realigned. It is worth noticing that the varying substrate structure obtained in previous work made leveling and identifying the underlying structure difficult already at an RMS value of $0.2 - 0.3nm$, this has been easier on HF-prepared substrates and makes the RMS roughness measurements more accurate and reproducible.

In conclusion LFO grow with a layer-by-layer growth mode with multiple layer nucleation until about 2.5nm where the growth reaches a threshold and transition into as 3D growth mode. The roughness increase earlier than for DI-treated substrates, but this is thought to be due to a different laser flux. The films are seen to be strained all the way through, although RHEED d-spacing show a large increase. An increased setpoint temperature leads to an increase in surface roughness and a break up of the film at $660°C$. This, in addition to previous work [17], suggests that optimal growth conditions of LFO in the (111)-orientation is achieved at lower temperatures than in (100)-oriented growth [36, 37].

4.3.2 Heterostructures - LFO/LSMO

In addition to the thin films grown with LSMO as a buffer layer, LFO thin films were also grown on a $30nm$ thick LSMO layer to investigate the growth mode on thicker and rougher LSMO. Growth of such heterostructures is still interesting as it allows for investigations of how LFO grow on thick and rough LSMO, compared to a thin buffer layer as in section 4.2.2.

LSMO Reference Layer In the reference film the RHEED intensity started out falling rapidly before increasing after about 200 pulses and then falling back, it then continued approximately constant (see figure 4.25a). RHEED oscillations were observed during the first 800 laser pulses, with a period of 19s. The oscillations damped out around 150 pulses ($\sim 2nm$), before the amplitude increased once more. During growth of the heterostructures a similar RHEED intensity development was also seen during LSMO deposition for the heterostructure with a $5nm$ thick LFO layer. However, for the two other heterostructures the RHEED intensity curve was observed to fall and then level out without the increase observed in the reference film (figure 4.25b). The RHEED oscillations were in this case observed for the first 900-1000 pulses with a period of 19 laser pulses.

The RHEED diffraction pattern from after deposition of the reference film show streaks which indicating a 3D surface (figure 4.25d), this was also observed already after about 300 laser pulses. Measurements collected from the AFM images of the thin film show an RMS roughness of $0.206nm$.

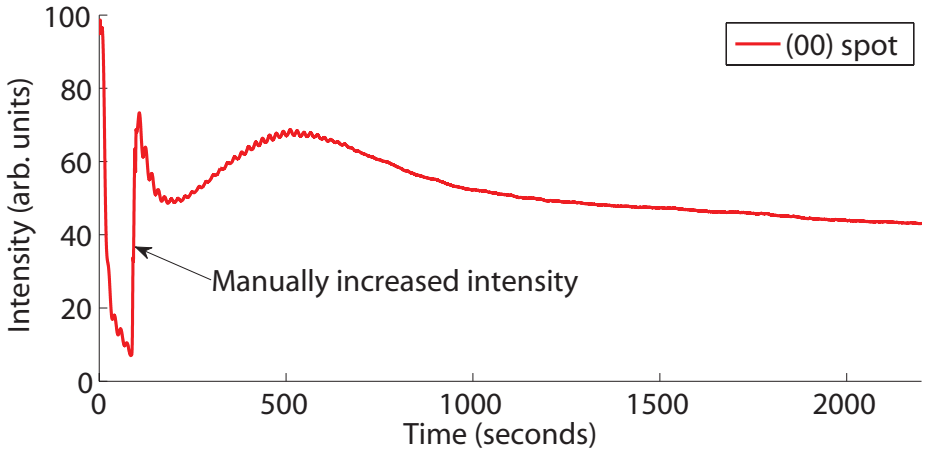

(a)

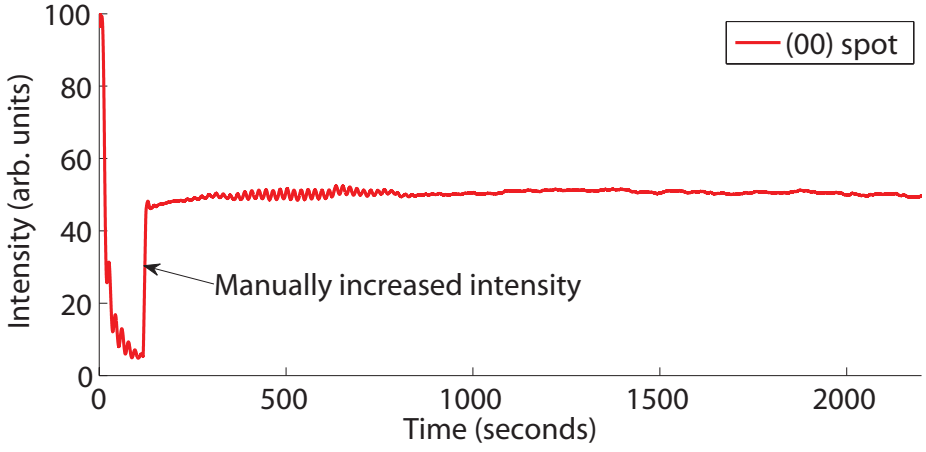

(b)

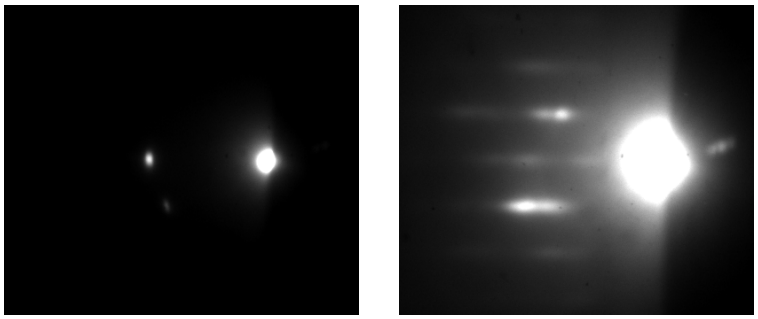

(c) (d)

Figure 4.25: RHEED intensity oscillations from deposition of LSMO on (111)-oriented STO and RHEED diffraction pattern from the film presented in (a). (a) Show the oscillations from the specular spot of the 30nm thick reference film. (b) Show the oscillations from the LSMO deposition of one of the heterostructures. (c) RHEED diffraction pattern before deposition for the sample in (a). (d) RHEED diffraction pattern after deposition for the sample in (a).

D-spacing oscillations were also observed during growth of LSMO. They were seen to have the same period as the RHEED intensity oscillations and a phase shift of approximately 180°. The oscillations were observed for approximately the first 1000 laser pulses or $15nm$ of the LSMO growth (figure 4.26). The d-spacing is first seen to drop to approximately the d-value of bulk LSMO, it then rises as the growth seems to enter a roughening period, before dropping once again. Then it starts increasing gradually, finally ending up at $5.49\mathring{A}$ at 2200 pulses or $30nm$. This is between the bulk value for STO ($5.52\mathring{A}$) and LSMO ($5.47\mathring{A}$) value for the in-plane lattice constant.

Rocking curve measurements showed a good crystalline quality with a FWHM of 0.024°. A $\omega - 2\theta$ scan of the LSMO reference film may be seen in figure 4.27 and show clear thickness fringes indicating high crystalline quality. The thickness is calculated to $24nm$ and the out-of-plane lattice parameter $d_{110} = 2.22\mathring{A}$. That means a 0.63% lower value than bulk LSMO ($2.24\mathring{A}$) indicating a compressive strain.

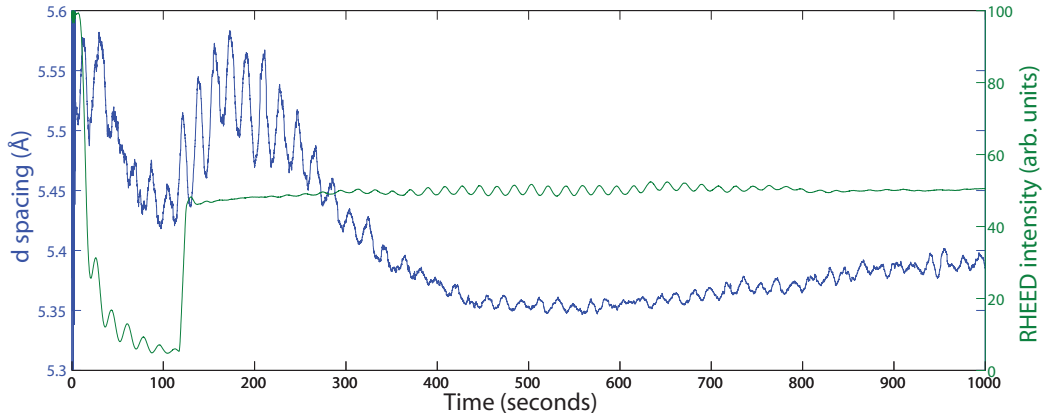

Figure 4.26: D-spacing and RHEED intensity oscillations for the first 1000 pulses during growth of LSMO (sample p30504).

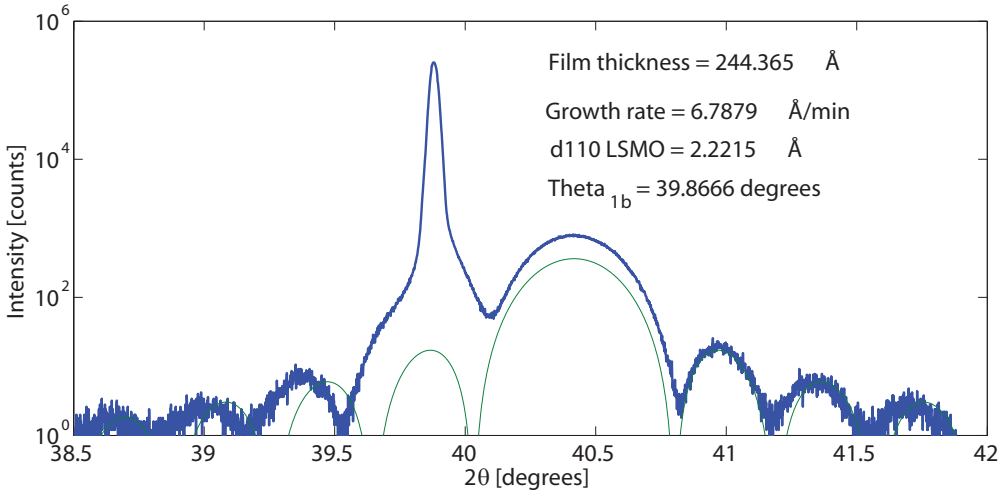

Figure 4.27: $\omega - 2\theta$ scan of 30nm thick LSMO thin film reference layer. The sharp peak is the STO (111) peak and the broader peak on the right is the LSMO (111) peak.

In-situ RHEED Studies From figure 4.28a it is seen that the RHEED specular intensity falls during the first few pulses, and then increase after about 130 pulses as the LFO layer gets thicker. RHEED intensity oscillations were not observed.

Upon depositing LFO on the LSMO layer, the d-spacing increases exponentially before settling more or less at a value of $6\mathring{A}$ after 1500 laser pulses, as may be seen in figure 4.30b.

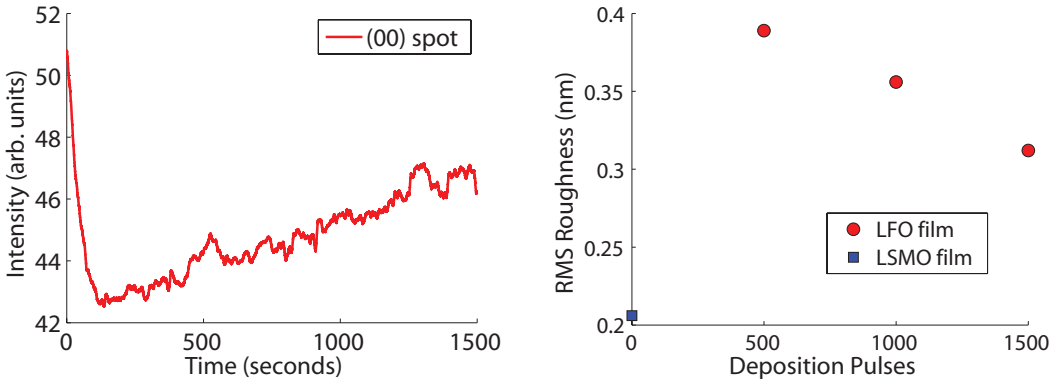

(a) (b)

Figure 4.28: (a) RHEED intensity from the specular spot during deposition of $7.5nm$ of LFO on a $30nm$ thick LSMO film and (b) RMS roughness of the grown heterostructures.

Surface Roughness The RMS roughness development of the deposited LFO thin films are illustrated in figure 4.28b and show an increasing roughness after initial deposition of LFO. However, the RMS roughness is then seen to decrease with thicker LFO films. The thin film surface is thus observed to get smoother with increased thickness, not rougher. AFM images of the thin films are presented in figure 4.29, and show that the substrate structure is difficult to observe in the thinnest film, but gets clearer as the LFO layer gets thicker.

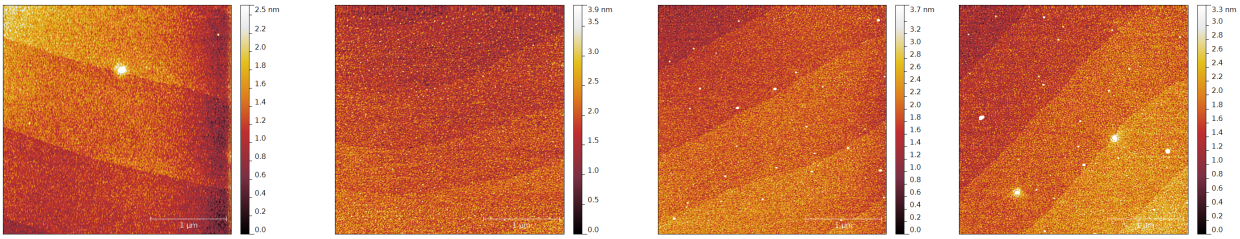

(a) (b) (c) (d)

Figure 4.29: 3x3um AFM images of (a) the LSMO($30nm$) reference layer and LFO/LSMO($30nm$) heterostructures. (b) $2.5nm$ LFO, (c) $5nm$ LFO and (d) $7.5nm$ LFO.

Crystallographic Characterization XRD measurements show a high crystalline quality for both the LSMO and the LFO layer. Rocking curves gave on average a 0.016° for the substrate STO peak, 0.027° for the LSMO peak and 0.026° for the LFO peak. The FWHM values are also tabulated in table 4.3. A $\omega - 2\theta$ scan of the heterostructure with the thickest LFO layer may be seen in figure 4.30a. The other LFO thin films were too thin to make a large impact on the $\omega - 2\theta$ scan and are therefore not shown. The out-of-plane pseudo-cubic (111) lattice parameter of the LFO layer is found to be $\sim 2.28\mathring{A}$, indicating a strained film. The fitting to the thickness fringes is difficult for LFO due to low intensity of the peaks as a result of the thin film.

Sample	Material	Thickness [nm]	RMS Roughness [nm]	FWHM (substrate) [°]
p30519	LSMO	30	0.206	0.024 (0.020)
p30502	LFO/LSMO	2.5/30	0.389	0.025/0.026 (0.014)
p30503	LFO/LSMO	5.0/30	0.356	0.022/0.023 (0.008)
p30504	LFO/LSMO	7.5/30	0.312	0.032/0.032 (0.027)

Table 4.3: Overview of LFO/LSMO heterostructures and a LSMO reference film.

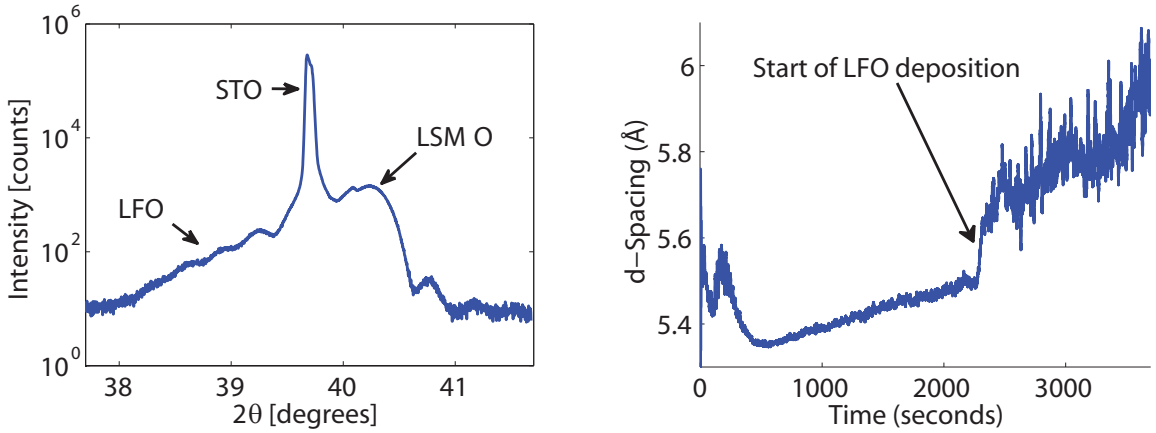

(a) (b)

Figure 4.30: (a) $\omega - 2\theta$ scan of a LFO($7.5nm$)/LSMO($30nm$) heterostructure grown on (111)-oriented STO substrates. (b) In-situ RHEED d-spacing curve from deposition of the heterostructure.

4.3.2.1 Discussion

The most important properties for the heterostructures are the crystalline quality and the growth at the LFO/LSMO interface. One of the most interesting observations in this section is the observation of increased RMS roughness for thicker LFO layers.

LSMO Reference Film The development of the surface roughness corresponds well to observation made by Hallsteinsen et al [11]. The damping of the RHEED intensity after around 100-200 pulses indicating a 3D growth mode around $1 - 2nm$ and the return of the oscillations then indicate a new 2D growth mode before it returns to 3D growth after around 900 pulses or $10 - 11nm$, corresponds well with figure 2.7 in section 2.3.2 reproduced from Hallsteinsen et al [11].

The LSMO thin film grown as a reference layer for the heterostructures showed an interesting development in the RHEED intensity curve (see figure 4.25a). A similar RHEED intensity development for a LSMO thin film have, by Boschker et al [50], been attributed to non-thermal growth whereas the development seen in figure 4.25b was identified as thermal growth. They report a depletion of Mn content during non-thermal growth, but not during thermal growth. The depletion of Mn is attributed to high adatom energies leading to a selective resputtering at the sample surface. The roughening transition is also seen to be delayed for thermal growth. The fact that both RHEED intensity tendencies are observed at identical parameters may indicate that we are at a boundary and only small variations in temperature, laser intensity, substrate distance or pressure might lead to a switch from nonthermal to thermal growth. However, in figure 4.31, streaking of the diffraction spots and multiple spots

appearing are observed. The neighboring diffraction spots may have influenced the RHEED intensity and cause the increase. The red circle in figure 4.25a represents the detection area for the RHEED intensity curve. It is more likely that this is the origin as streaking is seen in the red circle.

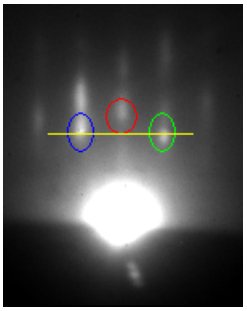

Figure 4.31: RHEED diffraction pattern after 375 pulses of deposited LSMO for the LSMO reference layer. The blue, red and green circles are is the detection spots of the RHEED intensity oscillations and the yellow line is the d-spacing detection line.

The RMS roughness of the sample film is $0.206nm$, which is lower than the $2.5nm$ thick LFO thin film. LFO thus grow in a rougher manner on (111)-oriented STO under these conditions.

The development of the d-spacing curve seen in figure 4.26 is interesting. The oscillations indicate a 2D island layer-by-layer growth mode, but the general development of the d-spacing is more peculiar. Generally, an increase in d-spacing is observed when the RHEED oscillations indicate that the film gets rougher. This is in agreement with Fuhr and Mullers [42] theory of angular dispersion of the electron beam as the origin of the oscillations in d-spacing. When the roughness is high it will result in larger islands and contributions from several open layers leading to an increased overall dispersion. The origin of the decrease in d-spacing may, on the other hand, be explained by the theory of Massies et al [41]. As LSMO has a smaller in-plane lattice constant, elastic relaxation at the edges would explain a fall in the d-spacing as the overall lattice constant would be smaller. It thus looks like a combination of the two theories needs to be applied in order to explain the evolution of the d-spacing.

It seems that the step density of the open layers leads to a change towards the relaxed value for the in-situ d-spacing at the surface. The fact that the XRD data show a strained film, however, indicate that this is a surface effect and that the film is strained as the layers are completed.

It should be noted that these theories are developed in order to explain the oscillations in the d-spacing curve and extending them to the general development for the d-spacing may have its limitations. It is done here in an effort to explain the observed changes in in-situ in-plane lattice constant at the surface.

Growth Mode As may be seen from the figure 4.29a, the LSMO layer morphology consists of 3D islands. A possible explanation for the initial roughening may be a difference in ES-barrier for the adatom at the LFO/LSMO surface compared to LFO/LFO growth. The growth of the first couple of monolayers of LFO may be influenced by the probability of interlayer transport and mobility of the adatoms when LFO grow on LSMO. The subsequent decline in surface roughness may then be explained by a lower ES-barrier and increased interlayer transport [46], as this would lead to the adatoms filling in the groves instead of creating new islands on islands. However, with growth at a 3D surface the data collected is not sufficient to make any conclusions and these are thus only speculations.

Strain Considering the d-spacing curve in figure 4.30a it looks like the in-plane lattice parameter relax both during deposition of LSMO and LFO. However, there are a lot of discrepancies in the development demonstrated by the curve.

The crystalline quality and development of the d-spacing of the reference film is discussed above and conclude that the in-plane lattice spacing of the LSMO layer is strained to the substrate. The XRD data from the LFO layer is not as good as for the LSMO layer due to the thin layer, but the in-plane lattice parameter seems to be strained to the substrate and LSMO layer since the out-of-plane parameter is (as for the $30nm$ LFO film) elongated by 0.44%. The increase of the d-spacing seen in figure 4.30a is attributed to the low peak intensity due to the rough surface. The line profile at this stage showed that it is not possible to identify the diffraction peaks and the increase is assumed to be the line trace function wandering towards the center peak in search of a peak and thus higher values (see figure 4.24).

To conclude, the heterostructures have a high crystalline quality and are believed to be strained to the substrate's in-plane parameter throughout both layers.

In conclusion Heterostructures with a 30nm LSMO and 2.5, 5.0 and 7.5nm LFO layers are synthesized showing high crystalline quality and a strained in-plane lattice constant. The surface morphology is seen to improve as more LFO is deposited after an initial increase in surface RMS roughness.

Chapter 5

Conclusion

The aim of this work has been to elucidate how the initial growth of (111)-oriented LFO was influenced by the substrate, comparing STO substrates and LSMO buffer layers. In addition, the governing growth mode was to be investigated. Epitaxial thin films were grown by PLD and characterized by AFM, in-situ RHEED and XRD measurements.

Smooth HF-treated substrates with a parallel step-and-terrace and a high crystalline quality was observed to yield higher quality thin films compared to DI-treated substrates and were therefore preferred in growth studies. LSMO did not grow well on DI-prepared substrates even though it has before, indicating that the optimal growth conditions may not be the same for DI- and HF- treated substrates.

Initially, LFO was seen to grow in a layer-by-layer growth mode on STO. Oscillations in both the RHEED intensity and the in the in-plane lattice constant (d-spacing) were observed during in-situ RHEED monitoring, this has been observed in (100)-oriented growth and indicated layer-by-layer growth. Two growth regimes were observed by RHEED during the first two monolayers, the first RHEED intensity peak was observed after half the number of laser pulses compared to the following RHEED oscillation period. The proposed origin for this observation was a filling of $Sr-$ vacancies at the assumed Ti^{4+} terminated interface.

Initial growth of LFO on LSMO buffer layers showed a different development as it had a constant RHEED oscillation period from the start of the deposition. RHEED oscillations and AFM images confirmed a layer-by-layer growth mode for thin growth on LSMO as well. Also, the increase in roughness was slightly less than for growth directly on STO and indicated a possible screening effect of the polar surface by the LSMO layer.

The continued growth of LFO on STO was also studied. The development of the RHEED oscillations and AFM images showed a 2D-3D transition after about $2.5 - 5.0nm$, indicating a transition from layer-by-layer to 3D island growth. However, the substrate structure was reflected in the thin films for all thin films, the thickest being 30nm. Also, XRD measurements showed a high crystalline quality and a strain in the LFO thin film throughout the the growth. Increasing the temperature lead to an increased roughness indicating that $540°C$ was a good choice of deposition temperature.

Heterostructures of LFO/LSMO were also grown in order to investigate the structural quality of such a structure. The $30nm$ thick LSMO layer had a layer-by-layer growth mode and showed roughness of $0.204nm$. Also during growth of LSMO d-spacing oscillations approximately 180° out of phase were observed confirming layer-by-layer growth. The surface roughness increased when depositing LFO, but fell as the LFO layer got thicker. This fall in surface roughness is attributed to filling of groves. The crystallographic measurements with XRD showed a strain in both the LSMO and the LFO buffer layer. Good crystalline quality was seen in FWHM values from rocking curve measurements.

A large change in d-spacing was observed by in-situ RHEED for all of the thin films, however XRD showed strained films. The large change in the in-plane lattice constant at the surface is thought to be a surface effect. It was attributed to an increased surface roughness leading to a general increase of the island density which affects the d-spacing.

Comparing the growth on HF-prepared substrates in this work with growth on DI-prepared substrates in previous work [17] the surface roughness was higher and the dependents of temperature comparable. This may, however, be due to change in growth conditions.

To conclude, LFO growth on both STO and LSMO resulted in an initial layer-by-layer growth mode. The first monolayer did however develop differently, with indications of a mixed first monolayer observed on STO and not on LSMO. Epitaxial growth of LFO has been achieved with a layer-by-layer growth mode transitioning into 3D island growth after $2.5nm$. The morphology then developed in a linear manner. Compared to LSMO growth where an initial roughening is observed followed by a new 2D growth regime, the LFO was observed to grow in a rougher manner. The decrease in surface roughness with thicker LFO layers in the heterostructures may indicate a smother growth of LFO on LSMO.

Chapter 6

Further Work

The results acquired in this work are only preliminary, and further studies are necessary. First of all, in order to fully understand the development of growth on STO, further studies including a larger variation of thicknesses will be needed. For example, in the curve describing the development of surface roughness a linear development may be observed between 2.5 and 7.5nm, but the rate of increase seems to fall when approaching 30nm.

It was indicated that LFO might grow smoother on the LSMO buffer layer due to a possible screening of the polar surface by the LSMO buffer layer. In order to confirm this theory more data is needed in order to determine how LFO growth on LSMO will develop after the first two monolayers.

Also, a study of how the growth modes and surface will be influenced by pressure, substrate-target distance and laser spot area would be interesting. Further investigations are also needed in order to be sure of the origin of the different growth regimes observed over the first two monolayers and weather this will happen at other interfaces too.

Last but not least, the characterization done in this work is purely structural and studies of the magnetic properties of LFO and the LFO/LSMO heterostructures will be a natural next step to investigate.

Bibliography

[1] G.E. Moore. "cramming more components onto integrated circuits", 1965.

[2] G.E. Moore. "progress in digital integrated electronics". In *Electron Devices Meeting, 1975 International*, volume 21, pages 11–13. IEEE, 1975.

[3] S. Borkar and A.A. Chien. "the future of microprocessors". *Communications of the ACM*, 54(5):67–77, 2011.

[4] W.J. Gallagher and S.S.P. Parkin. "development of the magnetic tunnel junction mram at ibm: From first junctions to a 16-mb mram demonstrator chip". *IBM Journal of Research and Development*, 50(1):5–23, 2006.

[5] W.H. Meiklejohn and C.P Bean. "new magnetic anisotropy". *Physical Review*, 102(5):1413, 1956.

[6] H.Y. Hwang, Y. Iwasa, M. Kawasaki, B. Keimer, N. Nagaosa, and Y. Tokura. "emergent phenomena at oxide interfaces". *Nature materials*, 11(2):103–113, 2012.

[7] X. Ke, M.S. Rzchowski, L.J. Belenky, and C.B Eom. "positive exchange bias in ferromagnetic lasrmno/ srruo bilayers". *Applied physics letters*, 84:5458, 2004.

[8] J. Chakhalian, A.J. Millis, and J. Rondinelli. "whither the oxide interface". *Nature materials*, 11(2):92–94, 2012.

[9] J. Mannhart and D.G. Schlom. "oxide interfaces - an opportunity for electronics". *Science*, 327(5973):1607–1611, 2010.

[10] L.W. Martin, Y.H. Chu, and R. Ramesh. "advances in the growth and characterization of magnetic, ferroelectric, and multiferroic oxide thin films". *Materials Science and Engineering*, 68(4-6):89–133, 2010.

[11] I. Hallsteinsen, J.E. Boschker, M. Nord, S. Lee, M. Rzchowski, P.E. Vullum, J.K. Grepstad, R. Holmestad, C.B. Eom, and T. Tybell. "surface stability of epitaxial la0.7sr0.3mno3 thin films on (111)-oriented srtio3". *Journal of Applied Physics*, 113(18):183512–183512, 2013.

[12] M. Gibert, P. Zubko, R. Scherwitzl, J. Íñiguez, and J-M. Triscone. "exchange bias in lanio3–lamno3 superlattices". *Nature materials*, 11(3):195–198, 2012.

[13] D.G. Schlom, S. Guha, and S. Datta. "gate oxides beyond sio2". *MRS bulletin*, 33(11):1017–1025, 2008.

[14] Y. Huai. "spin-transfer torque mram (stt-mram): Challenges and prospects". *AAPPS Bulletin*, 18(6):33–40, 2008.

[15] Y. Yamada, T. Kusumori, and H. Muto. "pinning effect of a lafeo3 buffer layer on the magnetization of a la1-xpbxmno3 layer". *Applied Physics Letters*, 80(8):1409–1411, 2002.

[16] V. Skumryev, S. Stoyanov, Y. Zhang, G. Hadjipanayis, D. Givord, and J. Nogués. "beating the superparamagnetic limit with exchange bias". *Nature*, 423(6942):850–853, 2003.

[17] J. V. Wasvik. "growth of lafeo3 on (111)-oriented srtio3 by pulsed laser deposition". Technical report, Norwegian University of Science and Technology, 2013.

[18] J. Nogués and I.K. Schuller. "exchange bias". *Journal of Magnetism and Magnetic Materials*, 192(2):203–232, 1999.

[19] X. Ke, L.J. Belenky, C.B. Eom, and M.S. Rzchowski. "antiferromagnetic exchange-bias in epitaxial ferromagnetic lasrmno/ srruo bilayers". *Journal of applied physics*, 97:10K115, 2005.

[20] J. Nogués, J. Sort, V. Langlais, V. Skumryev, S. Suriñach, J.S. Muñoz, and M.D. Baró. "exchange bias in nanostructures ". *Physics Reports*, 422(3):65 – 117, 2005.

[21] M. Ziese, I. Vrejoiu, and D. Hesse. "inverted hysteresis and giant exchange bias in lasrmno/srruo superlattices". *Applied Physics Letters*, 97:052504, 2010.

[22] A.J.H.M. Rijnders. *"The initial growth of complex oxides: study and manipulation"*. University of Twente, 2001.

[23] H.M. Christen and G. Eres. "recent advances in pulsed-laser deposition of complex oxides". *Journal of Physics: Condensed Matter*, 20(26):264005, 2008.

[24] G. Ehrlich and F.G. Hudda. "atomic view of surface self-diffusion: Tungsten on tungsten". *The Journal of Chemical Physics*, 44:1039, 1966.

[25] R.L. Schwoebel. "step motion on crystal surfaces. ii". *Journal of Applied Physics*, 40(2):614–618, 1969.

[26] A. Garg. "growth and characterization of epitaxial oxide thin films". 2001.

[27] J.L. Blok, X. Wan, G. Koster, D.H.A. Blank, and G. Rijnders. "epitaxial oxide growth on polar (111) surfaces". *Applied Physics Letters*, 99(15):151917–151917, 2011.

[28] A. Biswas, P.B. Rossen, C-H. Yang, W. Siemons, M-H. Jung, I.K. Yang, R. Ramesh, and Y.H. Jeong. "universal ti-rich termination of atomically flat srtio3 (001),(110), and (111) surfaces". *Applied Physics Letters*, 98(5):051904–051904, 2011.

[29] J. Chang, Y-S. Park, and S-K. Kim. "atomically flat single-terminated srtio3 (111) surface". *Applied Physics Letters*, 92(15):152910–152910, 2008.

[30] N. Nakagawa, H.Y. Hwang, and D.A. Muller. "why some interfaces cannot be sharp". *Nature materials*, 5(3):204–209, 2006.

[31] J. Chang, Y-S. Park, J-W. Lee, and S-K. Kim. "layer-by-layer growth and growth-mode transition of srruo3 thin films on atomically flat single-terminated srtio3 (111) surfaces". *Journal of crystal growth*, 311(14):3771–3774, 2009.

[32] J. Chang, J-W. Lee, and S-K. Kim. "layer-by-layer growth of srfeo3-delta thin films on atomically flat single-terminated srruo3/srtio3 (111) surfaces". *Journal of Crystal Growth*, 312(4):621–623, 2010.

[33] J. Li, J. Wang, M. Wuttig, R. Ramesh, N. Wang, B. Ruette, A.P. Pyatakov, A.K. Zvezdin, and D. Viehland. "dramatically enhanced polarization in (001),(101), and (111) bifeo3 thin films due to epitiaxial-induced transitions". *Applied physics letters*, 84:5261, 2004.

[34] J.E. Boschker. *"Control of surface quality and structural distortions in perovskite oxide thin films"*. PhD thesis, Norwegian University of Science and Technology, Department of Electronics and Telecommunications, 2012.

[35] J. Feng, X. Zhu, and J. Guo. "reconstructions on srtio3 (111) surface tuned by ti/sr deposition". *Surface Science*, 2013.

[36] E. Folven. *"Antiferromagnetic Domain Structure in LaFeO3 Thin Films and Nanostructures"*. Doktoravhandlinger ved NTNU. Norwegian University of Science and Technology, 2011.

[37] J.W. Seo, E.E. Fullerton, F. Nolting, A. Scholl, J. Fompeyrine, and J-Pierre. Locquet. "antiferromagnetic lafeo3 thin films and their effect on exchange bias". *Journal of Physics: Condensed Matter*, 20(26):264014, 2008.

[38] R. Eason. *"Pulsed laser deposition of thin films: applications-led growth of functional materials"*. Wiley-Interscience, 2007.

[39] Ayahiko I. and P.I. Cohen. *"Reflection High-Energy Electron Diffraction"*. Cambridge University Press, 2004.

[40] W. Braun. *"Applied RHEED: reflection high-energy electron diffraction during crystal growth"*, volume 154. Springer Verlag, 1999.

[41] J. Massies and N. Grandjean. "oscillation of the lattice relaxation in layer-by-layer epitaxial growth of highly strained materials". *Physical review letters*, 71(9):1411–1414, 1993.

[42] J.D. Fuhr and P. Muller. "physical origin of in-plane lattice spacing oscillations measured by reflection high-energy electron diffraction during epitaxial growth". *Physical Review B*, 84(19):195429, 2011.

[43] R. Waser. *"Nanoelectronics and information technology"*. Wiley-Vch, 2012.

[44] S.I. Csiszar. *"X-ray Diffraction and X-ray Absorption of Strained CoO and MnO Thin Films"*. MSC Ph.D.-thesis series. 2005.

[45] G. Haugstad. *"Atomic Force Microscopy: Understanding Basic Modes and Advanced Applications"*. Wiley, 2012.

[46] M.G. Lagally and Z. Zhang. "materials science: Thin-film cliffhanger". *Nature*, 417(6892):907–910, 2002.

[47] P. Müller, P. Turban, L. Lapena, and S. Andrieu. "elastic relaxation during 2d epitaxial growth: a study of in-plane lattice spacing oscillations". *Surface science*, 488(1):52–72, 2001.

[48] J.E. Boschker and T. Tybell. "qualitative determination of surface roughness by in situ reflection high energy electron diffraction". *Applied Physics Letters*, 100(15):151604–151604, 2012.

[49] G. Rijnders, D.H.A. Blank, J. Choi, and C-B. Eom. "enhanced surface diffusion through termination conversion during epitaxial srruo3 growth". *Applied physics letters*, 84(4):505–507, 2004.

[50] J.E. Boschker, E. Folven, Å.F. Monsen, E. Wahlstrom, J.K. Grepstad, and T. Tybell. "consequences of high adatom energy during pulsed laser deposition of la0. 7sr0. 3mno3". *Crystal Growth and Design*, 12(2):562–566, 2012.